Fall 2021

Pulsed Laser Annealing on the Optoelectronic Properties of ZnO Thin Films

Md Abu Zobair
Missouri State University, Zobair007@live.missouristate.edu

PULSED LASER ANNEALING ON THE OPTOELECTRONIC PROPERTIES OF ZnO THIN FILMS

A Master's Thesis

Presented to

The Graduate College of

Missouri State University

In Partial Fulfillment

Of the Requirements for the Degree

Master of Science, Material Science

By

Md Abu Zobair

December 2021

PULSED LASER ANNEALING ON THE OPTOELECTRONIC PROPERTIES OF ZnO THIN FILMS

Physics, Astronomy, and Materials Science

Missouri State University, December 2021

Master of Science

Md Abu Zobair

ABSTRACT

ZnO thin films have attracted great attention recently due to their unique electronic and optical properties. However, for proper implementation of ZnO in electronic devices it is necessary to understand the role of native point defects present inside the material as these wide bandgap semiconductors are inherently n-type due to oxygen vacancies. The objective is to control the electronic and optical properties of ZnO thin films through pulsed laser annealing (PLA). Thin films of ZnO have been grown on different substrates using pulsed laser deposition. Then PLA of the films are done by changing laser parameters (energy, frequency, pulse width, number of shots). Structural quality of the annealed films is investigated using X-ray diffraction, electron microscopy, Raman spectroscopy. Optoelectronic properties of the PLA films are investigated using photoluminescence spectroscopy and electrical characterization. It was shown from the experimental results that the conductivity can be changed through the modification of point defects (vacancies and interstitials) with the selection of proper annealing parameters. The photoluminescence spectroscopy showed for a controlled number of laser shots and energy, peak intensities associated with defects (vacancies and interstitials) are decreased while area of band emission peaks increased. Additionally, the structural properties of annealed ZnO by simulating the PLA process through MD simulation were investigated. The results were also further evidence that laser irradiation can be a useful technique for semiconductor material modification.

KEYWORDS: pulsed laser annealing, thin films, ZnO, semiconductor defects, photoluminescence, electrical conductivity, molecular dynamic simulation

PULSED LASER ANNEALING ON THE OPTOELECTRONIC

PROPERTIES OF ZnO THIN FILMS

By

Md Abu Zobair

A Master's Thesis
Submitted to the Graduate College
Of Missouri State University
In Partial Fulfillment of the Requirements
For the Degree of Master of Science, Material Science

December 2021

Approved:

Kartik C Ghosh, Ph.D., Thesis Committee Chair

Robert A Mayanovic, Ph.D., Committee Member

Tiglet Besara, Ph.D., Committee Member

Julie Masterson, Ph.D., Dean of the Graduate College

ACKNOWLEDGEMENTS

At First, I would like to thank the Almighty for giving me the opportunity to complete this research work successfully.

I am highly thankful to Dr. Ghosh for his continuous support and guidance. I have learned how to conduct a graduate level research work under his supervision during my MS degree at Missouri State University. I would also like to thank Dr. Robert A Mayanovic and Dr. Tiglet Besara for being in my thesis committee and sharing their insightful comments. My sincere thanks also go to my colleague Bishwajite Karmakar and my friend Fuad Nur Taufique.

I would like to thank my parents Abu Talib and Shahida Yasmin for their sacrifices and blessings. My special thanks go to my wife Mithila Mohammad for her patience. I dedicate this work to my daughter Alia Muntaha.

TABLE OF CONTENTS

LIST OF TABLES

LIST OF FIGURES

INTRODUCTION

Background

ZnO as a semiconductor material is a very promising and exciting aspect in electronic devices. It has direct and wide band-gap in the near-UV spectrum and has a large exciton binding energy. ZnO has Wurtzite hexagonal crystal structure, which is identical to another widely used material, GaN, but the ZnO is available in large bulk single crystals, and over the last few years the quality of ZnO single crystal substrates and thin films have improved a lot. GaN grown on sapphire has a high concentration of defects (10^6-10^9 cm^{-2}) due to large lattice mismatch of ~16%. On the other hand, the epitaxial growth of ZnO in different substrates have lower defect concentration and, hence can have better performance in electronic and photonic devices. Besides, ZnO is suitable for wet chemical etching, which gives it another edge over GaN in device design and fabrication[1, 2].

The crystal structures of ZnO are wurtzite, zinc blende, and rocksalt (Fig 1.1). Like other group II-VI compound semiconductors, ZnO crystalizes in either cubic zinc blende or hexagonal wurtzite structure where each anion is surrounded by four cations and vice versa. It has the typical tetrahedral sp^3 covalent bonding nature, but due to substantial ionic character, the bandgap tends to increase beyond what is expected from a covalent bonding. Under ambient condition, the thermodynamically stable phase is the wurtzite crystal structure, with lattice parameters a=3.24 Å and c=5.21 Å. Its bulk modulus is 142 GPa. Bulk ZnO undergoes a transition to the rocksalt phase at a pressure of ~9 GPa[3]. Room-temperature Raman scattering spectra showed transverse optical phonons at 378 cm^{-1} (A1) and 410 cm^{-1} (E1), longitudinal optical (LO) phonons at 576 cm^{-1} (A1) and 588 cm^{-1} (E1), and E2 phonons at 98 cm^{-1} (low) and 438 cm^{-1} (high)[4]. Due to spin orbit and crystal-field splitting, the valence band splits into three

levels at the center of the Brillouin zone, resulting in A, B, and C excitons. The A free exciton is the one with the lowest energy. Photoluminescence (PL) measurements showed that the A free exciton has a binding energy of 60 meV and that the band gap at 10 K is 3.437 eV.

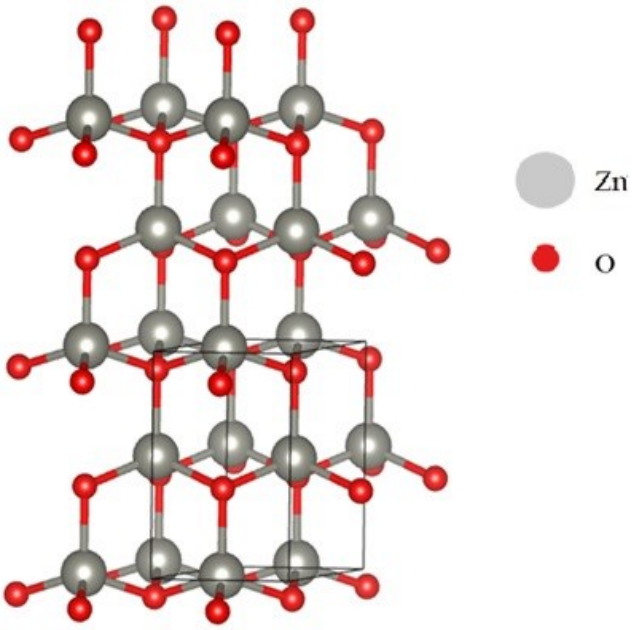

Fig 1.1: The wurtzite ($P6_3mc$ [186]) phase of ZnO. It's lattice parameters are a = b= 3.24 Å, c = 5.21 Å, $\alpha = \beta = 90^0$, and $\gamma = 120^0$.

Since the early days of semiconductor, the property, and characteristics of ZnO have been studied intensively, but the use of ZnO in electronic devices has been impeded by the lack of control on its electronic properties, which is mainly due to its defects. Even a very small number of defects and impurities (down to 10^{-14} cm^{-3}) can have significant effect on electrical and optical properties of semiconductors. ZnO is inherently n-type, the cause of which is still a matter of research and debate. With the recent success of nitrides in optoelectronics, the prospect of using

ZnO as an alternative has driven many researchers to work intensively on its semiconductor properties. One of the major efforts in this area is to control the unintentional n-type conductivity and thus achieve the p-type conductivity in ZnO. According to Liu *et al*., the oxygen vacancies in ZnO are actually +2 charged and thus responsible for the unintentional n-type conductivity, also for the non-stoichiometry of ZnO. First Principles calculations based on Density Functional theory (DFT) have also showed that native point defects are responsible for the unintentional n-type conductivity in ZnO. Obtaining p-type doing is also another aspect which is hindered by the defects as they play as compensating centers. Therefore, to control the electronic conductivity of ZnO it is very necessary to understand the role of native point defects (vacancies, interstitials and antisites)[15].

Defects in ZnO

Vacancy defects are empty lattice sites that would be filled in a pure crystal. If a neighboring atom moves in to take the empty site, the vacancy shifts in the opposite direction of the migrating atom's previous location. The surrounding crystal structure's stability ensures that nearby atoms will not collapse around the vacancy. Because they are attracted by atoms in the vicinity, nearby atoms in some materials migrate away from a vacancy[6]. Atoms that occupy a location in the crystal structure where there is usually no atom are known as interstitial defects. In general, they are high-energy arrangements (Fig: 1.2).

O vacancies, for example, have low formation enthalpies in p-type ZnO and are hence expected to form quickly. At normal temperature, O vacancy is a deep donor, but Zn interstitials

are unstable. In n-type ZnO, Zn vacancies act as compensatory acceptors. Other natural defects with high formation energies include Zn antisites, O antisites, and O interstitials[7]. They are unlikely to be found in high quantities in normal conditions, yet O interstitials may play a role in O self-diffusion. O vacancies, Zn interstitials, and Zn vacancy–Zn interstitial couples were identified using optically detected magnetic resonance.

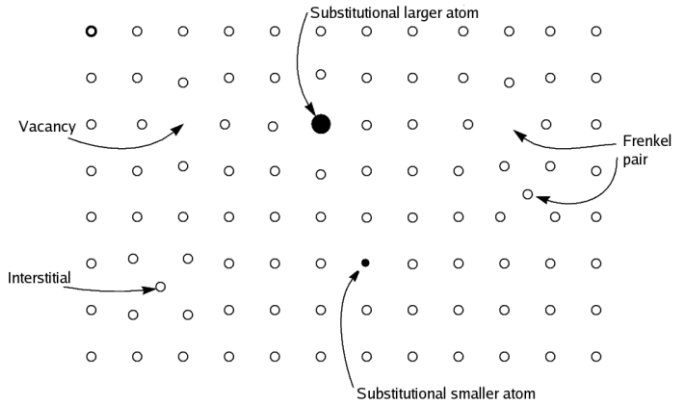

Fig 1.2: Native point defects in a crystal (Courtesy: Wikipedia of crystallographic defect)

The Zn interstitials are shallow donors, with a g-factor of g~1.96 for their "effective mass" (EM). At a temperature of 170 K, they anneal out. Zn interstitials are likewise shallow donors, according to first-principles calculations. They are rapid diffusers with migration barriers as low as 0.57 eV in n-type ZnO and have high formation energies. As a result, Zn interstitials are not stable at room temperature, as demonstrated by Vlasenko and Watkins' experiments. Positron annihilation measurements refuted the idea that Zn interstitials create n-type conductivity, showing that annealing in Zn vapor did not result in a decrease in Zn vacancies. If Zn interstitials had diffused into the crystal, the open-volume defects should have been filled by now. Instead, the scientists theorized that Zn vapor increased O vacancies in the bulk by causing

new ZnO to develop on the surface. While it is well agreed that Zn interstitials are unstable, complexes comprising N impurities and Zn interstitials have been proposed as stable, shallow donors[8].

The O vacancy is a deep, negative-U donor, with the 1+ charge state being thermodynamically unstable, according to first-principles calculations. The defect is in the neutral charge state when the Fermi energy is above the "0/2+ level." The defect has a charge of +2e when the Fermi energy is below the 0/2+ threshold. The O vacancy's 0/2+ level was calculated to be 0.5–0.8 eV higher than the valence-band maximum. The 0/2+ level was predicted to be 1–2 eV below the conduction-band minimum in calculations that attempted to adjust for the band gap error of the local density approximation. The migration barrier for the neutral O vacancy has been calculated to be 2 eV. O vacancies in n-type ZnO are a point of debate among theorists. Lany and Zunger, anticipated concentrations of 1017 cm^{-3} or more, although Janotti and Van de Walle argued that the formation energy is far too high for significant concentrations to exist at equilibrium[9]. Electron paramagnetic resonance is a phenomenon that occurs when electrons interact with one another. EPR experiments on electron-irradiated ZnO demonstrate that low-temperature illumination converts neutral O vacancies to the 1+ charge state. Due to an excited-to-ground state transition, the green luminescence band centered around 2.4 eV (510) nm has been attributed to O vacancies. Annealing in O_2 or Zn vapor creates 2.35 and 2.53 eV PL lines, respectively, but annealing in ZnO powder eliminates both lines. According to these findings, the 2.35 eV emission is caused by Zn vacancies, while the 2.53 eV emission is caused by O vacancies.Zn vacancies are double acceptors. The 0/1– and 1–/2– acceptor levels, according to first-principles calculations, are 0.1–0.2 and 0.9–1.2 eV above the valence-band maximum, respectively. Zn vacancies can be converted to the 1– or neutral charge

state under low-temperature illumination. Evans et al calculated that the ground state for the 1– charge state is 0.9 eV above the valence band based on the wavelength of light necessary to pump Zn vacancies from the 1– to the neutral charge state. Green fluorescence in some ZnO samples could be due to Zn vacancies. The transition from a shallow donor level to the 1–/2– acceptor level, as discussed by Janotti and Van de Walle, could result in PL approximately 2.5 eV. In addition, exposing ZnO samples to H plasma lowered the intensity of the green fluorescence, which is consistent with Zn vacancy passivation[10]. Despite the creation of defects such as Zn vacancies, electron irradiation causes a decrease in green fluorescence. The energy band diagram is shown in Fig 1.3.

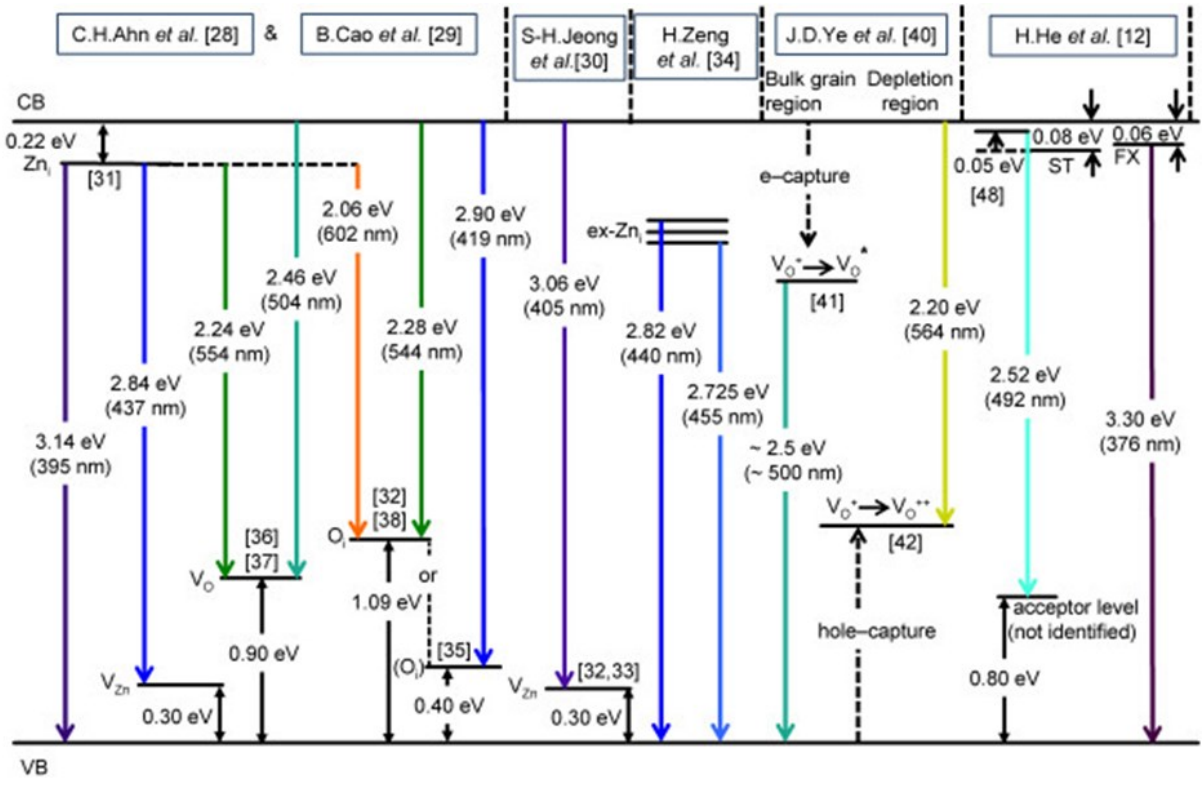

Fig 1.3: Some of the major defect levels in ZnO are depicted in the energy level diagram (CB stands for conduction band, VB for valence band, FX for free exciton, and ST for surface trap). Courtesy[11]

Pulsed Laser Annealing

In the last five years, a new discipline of materials science called directed energy processing has evolved for the processing and modification of semiconductor surface layers. The surface is heated using directional energy sources such as lasers or electron beams. These beams' unique temporal and spatial control overheat flow allows for the development of completely new structures and alloys. Surface layers, for example, can be melted and hardened in a matter of seconds to create metastable alloys. The incident beams can only modify the size of the layers that are required by Si integrated circuit technology. The first demonstrations of the utility of directed energy processing came from the annealing of implantation damage using lasers. Thus, the term laser annealing was coined. It is something of a misnomer, as most of the annealing mechanisms are in fact due to liquid or solid phase recrystallization. The field has progressed far beyond the annealing of implantation damage, and it is possible to recrystallize amorphous or polycrystalline Si on amorphous substrates by laterally sweeping a Si melt puddle with a moving laser or particle beam. Very large grains or even single-crystal Si can be produced by this technique, which may lead to a new generation of devices[12].

The facility of rapidly heating and cooling surface layers without heating the bulk depends on the pulse duration time t_p and the coupling depths of the heat source. For Q-switched solid state lasers the output pulses range from 10^{-9} to 10^{-7} sec, whereas for mode-locked lasers pulses as short as 10^{-12} sec can be generated. The cooling or quench rates of the surface layers using these pulsed sources will be in the range 10^{9}-10^{14} K/sec. Longer irradiation times can be achieved by the use of continuous sources with scanned spots. The fastest irradiation times will be 10^{-5}-10^{-6} sec, with cooling rates less than 10^{9} K/sec. The coupling of lasers to materials is very sensitive to the laser wavelengths and the state of the material[13]. On the other hand, the coupling,

or energy loss, of electron beams to solids does not depend, for all practical purposes, on the state of the material but is just a simple function of the incident energy. The temperature rise resulting from a surface heat source induced by a laser is given by following equation

$$T(t_p) - T_0 = F_d \frac{2\sqrt{t_p}}{\sqrt{\pi K \rho C_V}}$$

where K, ρ and C_v are the thermal conductivity, density, and heat capacity respectively. The initial temperature is denoted by T_0. F_d, the power flux deposited into the material, is a square pulse in time. The temperature rises as one-half power of the pulse width, a generic character of heat diffusion[14].

Shining a laser with wavelength λ perpendicularly onto the sample surface, the reflection coefficient can be expressed as,

$$r = \frac{n-1}{n+1}$$

where the refractive index $n = \sqrt{\varepsilon}$. The Drude model is quite adequate in infrared, which gives

$$\varepsilon = 1 - \frac{\omega_p^2}{\omega^2 + i\omega\omega_\tau}$$

The plasma frequency $\omega_p^2 = n_e e^2/m\varepsilon_0$, and the collision frequency $\omega_\tau = n_e e^2/m\,\sigma(T)$. The electron density n_e inside ZnO is roughly $1.54 \times 10^{22}/cm^3$. Electrical conductivity σ is temperature dependent. From energy conservation, the flux into ZnO has the form $F_d=(1-|r|^2)I_0$. Here, I_0 is the laser irradiance. In the frequency region, $\omega_\tau << \omega << \omega_p$. So, the Drude model gives[15]

$$F_d \approx \frac{2\omega_\tau}{\omega_p} I_0$$

Using these equations, surafce temparature rise was determined for laser irradiation upto 50 ps (Fig 1.4).

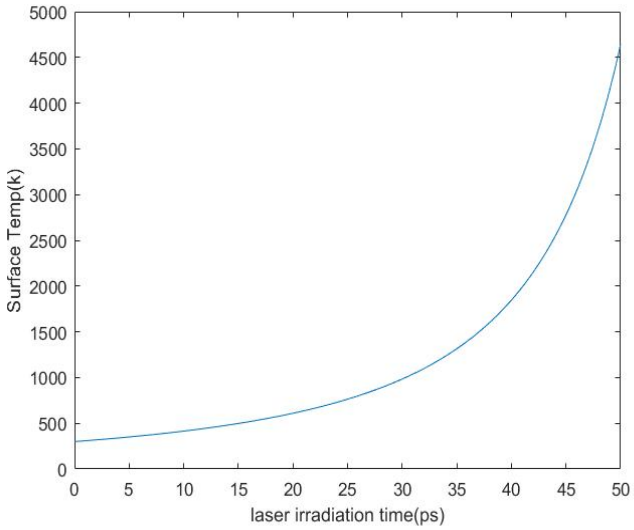

Fig 1.4: Pulsed temperature rise in ZnO surface for a 6ps laser pulse, 256 nm wavelength (Generated with MATLAB)

Objectives

My thesis focuses on the control of the native point defects in ZnO thin films with laser irradiation. The Laser irradiation technique that I will use is Pulsed Laser Annealing. In this process, surface of the thin films grown on different substrates with Pulse Laser Deposition technique will be exposed to laser pulses of short duration (10 ns). A recrystallization in the surface level is desirable, since the Laser energy is directly processed and the cooling rate is greater than the diffusion rate. My expectation is that, after annealing with this process, due to recrystallization, the point defects should decrease. At first, the role of native point defects and the Pulsed Laser Annealing will be discussed. Then the growth and characterization of the ZnO thin films will be discussed. And, in the next step, annealing and analysis of the data presented in this thesis will be discussed. In the last step, the MD simulation results will be discussed to understand the structural changes during annealing**.**

SYNTHESIS OF ZnO THIN FILM VIA PULSED LASER DEPOSITION

Without contamination from the substrate or thermal mismatch, ZnO thin films can be epitaxially produced with fewer defects. This is significant because the crystalline quality of the film has an impact on the performance of optoelectronic devices. Optimized growing and processing environments (pressure and temperature) are required for use in electrical and optoelectronic devices. Pulsed laser deposition (PLD), chemical vapor deposition (CVD), metal-organic CVD (MOCVD), and molecular-beam epitaxy (MBE), as well as sputtering, are some of the current techniques that provide for this level of control. Magnetron sputtering is the most scalable approach, however it comes at the cost of lower crystalline quality, which frequently results in columnar structures. The inferior crystalline quality of ZnO films generated by sputtering techniques is most likely due to difficulty regulating particles falling on the film surface, which prevents the formation of defect-free, high-quality films[16]. The technology of PLD is more effective in producing high-quality thin films of metal oxide materials. The plasma created by pulsed laser ablation has a high energy level, and its mobility may be easily controlled by altering processing parameters. PLD technology has been widely used for the creation of high-quality thin films for these practical reasons. A schematic of a PLD chamber is shown in Fig 2.1.

In the PLD method a high-power laser beam is focused inside a vacuum chamber to impact a known-composition target, resulting in a highly directed plume of gas material that condenses onto a substrate. Sintered ceramic disks manufactured from high-purity pressed powders, ZnO single crystals, and pure Zn with a reactive oxygen environment are utilized as targets for producing ZnO films by PLD. Glass and single-crystal substrates have both been used to create ZnO thin films via PLD, with the latter yielding the greatest results. Due to the large

area of single-crystal wafers and inexpensive cost, sapphire has been the most used substrate. Other single-crystal substrates, such as Si, GaAs, InP, CaF_2, and $LiTaO_3$, have also been used to produce ZnO using PLD[17].

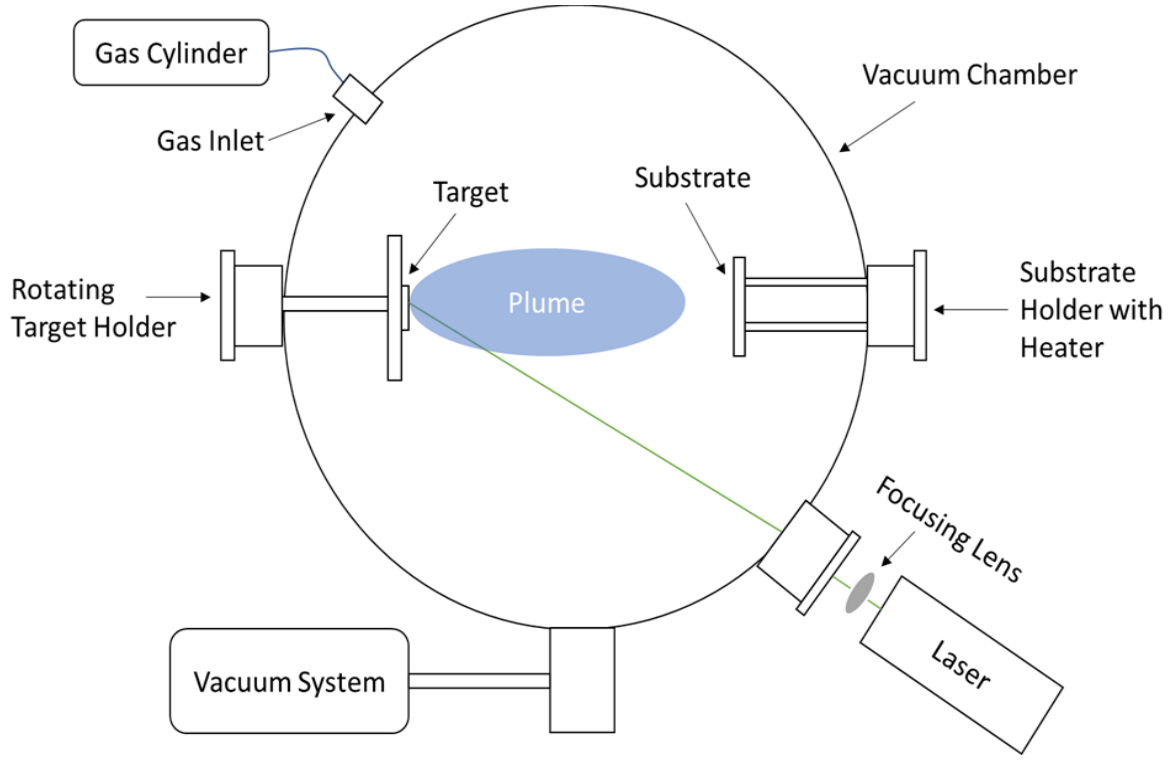

Fig 2.1: Schematic of a PLD Chamber. Vacuum chamber consists of gas inlet valve, focusing lens, port with quartz window, substrate holder/heater, pressure gauge, target holder/carousel, roughing pump, and turbomolecular pump.

For our experiment, we used Q-switched solid state laser with wavelength 256 nm and pulse width of 10 ns. For target material we have used high purity Zn Target. We have used two different substrates to grow ZnO, the first is Si (111) and the second one is Si/SiO_2 (400). By manipulating process parameters such as laser energy density, oxygen pressure, and substrate

temperature, we were able to create reasonably good quality ZnO thin films by laser ablation of Zn targets in an oxygen active atmosphere.

At first the substrates were rinsed in acetone with ultrasonic vibration for 20 min and then rinsed in ethanol before putting into vacuum chamber for deposition. The vacuum chamber of the deposition system was evacuated by the roughing pump and then with the turbomolecular pump down to 1.9×10^{-5} mbar. We chose different processing environments (pressure and temperature) for different substrates. For Si substrate, when the base pressure reached to the desired value, the substrate is heated to 400^0C, ramp time was controlled with a temperature controller. Then O_2 gas was introduced into the chamber and the pressure was increased to 1.9×10^{-2} mbar. The pressure was controlled to this point throughout the process. The distance between target and substrate was kept between around 5 cm. The Zn target is cleaned with 500 shots, then ablated with 40,000 shots from a neodymium-doped yttrium aluminum garnet (ND:YAG) nanosecond pulse laser with an average laser energy of 41 mJ/pulse. The pulse frequency was set at 10Hz with a Q-switch delay of 10s, and the laser energy density was around 3.1mJ/cm2. After depositing for approximately 1 hour, a thin film of ZnO was created on the top layer of the Si substrate. The sample is cooled to room temperature after deposition. For Si/SiO_2 substrate, same procedure as above was followed. This time the substrate temperature was raised to 600^0C and the O_2 pressure was increased further, kept at 1.5×10^{-1} mbar.

RESULTS & DISCUSSIONS

MD Simulation Studies Towards Rapid Annealing of ZnO

One of the aspects of the pulsed laser annealing (PLA) is that it is possible to achieve amorphous structures due to the rapid heating and cooling process. This process is similar to a melt/quench procedure and can be utilized to make thin amorphous(a)-ZnO films. We studied if ZnO can form a bulk glass state using the melt/quench process. These findings will aid in the development and understanding of thin a-ZnO films. Because experimental structural data on a-ZnO is few, theoretical modeling can shed light on the material's potential density and structure. Recent improvements in Sb phase change memory, where molecular dynamics (MD) melt/quench simulations have revealed insights into how successful Sb amorphization attempts can be, illustrate the success of such a method[18].

3D bulk of Amorphous ZnO structures were generated using MD simulations and the LAMMPS code to model the structure inside thin oxide films grown on substrates. We used the reaxff potential file, which allows continuous bond formation/breaking. ReaxFF is a complex force field with many parameters, so the computational cost is expected to increase. To minimize the cost, the simulation was done in Google cloud compute Engine, a virtual linux based cluster platform, which allows to run MD/DFT simulations.

a-ZnO structures were generated in an NPT ensemble using the following procedure: (i) equilibration of the system for 50 ps at 300 K; (ii) temperature was linearly increased to 2500 K (melting point of ZnO is ~2200 K) for 50 ps; (iii) the system was equilibrated for 500 ps at 2500 K; (iv) structures were cooled down to 300 K with a Cooling rate of 100 Kps−1; (v) the system was equilibrated for 50 ps at 300 K. The script from the input file is given below:

```
# REAX potential for ZnO system
units real
atom_style charge
read_data data.ZnO
pair_style reax/c lmp_control
pair_coeff * * ffield.reax.ZnOH Zn O
neighbor 2 bin
neigh_modify every 10 delay 0 check no
velocity all create 300 4928459 dist gaussian
#dump: output file
dump         1 all custom 100 dump_glass_rt_info.xyz id type x y z q fx fy fz
dump         2 all xyz 100 glass_eq_npt.xyz
dump         3 all xtc 100 test.xtc
timestep 0.5        #femtosecond
fix             1 all qeq/reax 1 0.0 10.0 1e-6 param.qeq
# ---------- STEP 1 : equilibrate at  300K----------------
fix             2 all npt temp 300.0 300.0 100 iso 1.0 1.0 100
thermo 1000
thermo_style    custom step temp epair etotal press vol density lx ly lz
run             100000
unfix           2
# ---------- STEP 2 : anneal it up to 2500K----------------
fix             3 all npt temp 300.0 2500.0 100 iso 1.0 1.0 100
#fix            6 all temp/rescale 100 5000 5000 5 1.0
thermo 1000
thermo_style    custom step temp epair etotal press vol density lx ly lz
run             100000
unfix           3

# ---------- STEP 3 : equilibrate at  2500K----------------
fix             4 all npt temp 2500.0 2500.0 100 iso 1.0 1.0 100
#fix            6 all temp/rescale 100 5000 5000 5 1.0
```

```
thermo 10000
thermo_style    custom step temp epair etotal press vol density lx ly lz
run             1000000
unfix           4
# ---------- STEP 4 : cool it down to 300K-quench----------------
fix             5 all npt temp 2500.0 300.0 100 iso 1.0 1.0 100
thermo 1000
thermo_style    custom step temp epair etotal press vol density lx ly lz
run             94000
unfix           5
# ---------- STEP 5 : equilibrate it at 300K----------------
fix             6 all npt temp 300.0 300.0 100 iso 1.0 1.0 100
thermo 1000
thermo_style    custom step temp epair etotal press vol density lx ly lz
run             1000000
```

The data file containing the coordinates of 2048 atoms of ZnO was created with the OVITO, an open visualization tool that is used create and visualize atomic structures for molecular simulations. The output file of the simulation was also visualized with OVITO and used to analyze the amorphous state of ZnO (Fig 3.1-2).

From the output files, the number of defects was analyzed using the Wigner-Seitz defetct analysis tool. Initially at 300 K in the stable structure there were ~200 vacancies and same amount of interstitials, which is the ideal condition. After annealing to 300K from 2500K, the number of defects also incresed which was ~750 vacancies and same amount of interstitials.

Coordination analysis was done in OVITO and RDF of the both states were determined (Fig 3.3). From the RDF, the per-atom coordination number was found for the c-ZnO around 1000 and for the a-ZnO around 720. It is evident from the RDF that probability of finding a bonding atom pair decreases as the pair separation distance increases for amorphous structure.

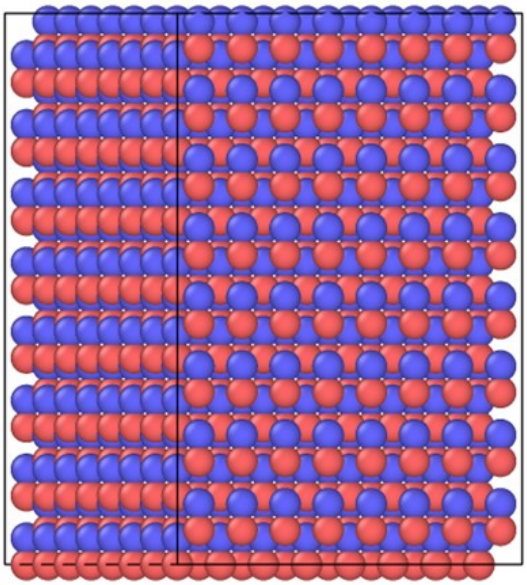

Fig 3.1: ZnO bulf of 2048 atom at room temperature, 300 K (created with Ovito)

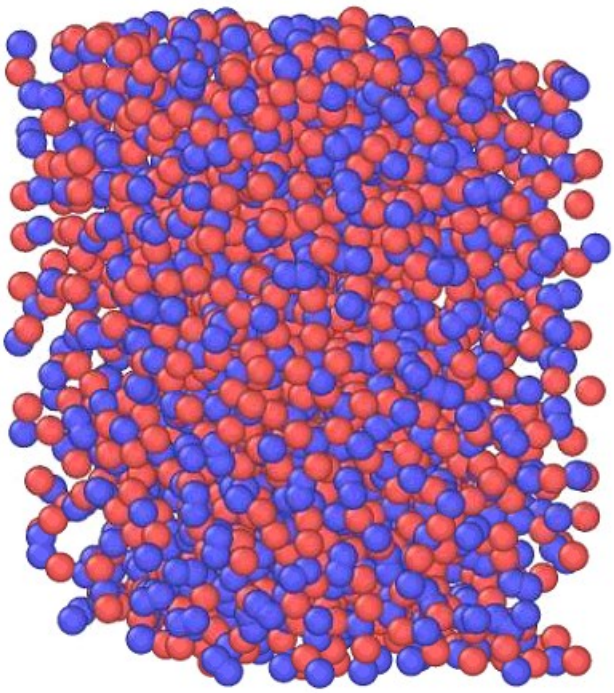

Fig 3.2: The amorphous state of Bulk ZnO, stabilized at 300K after annealing from 2500K in a cooling rate of 100K/ps

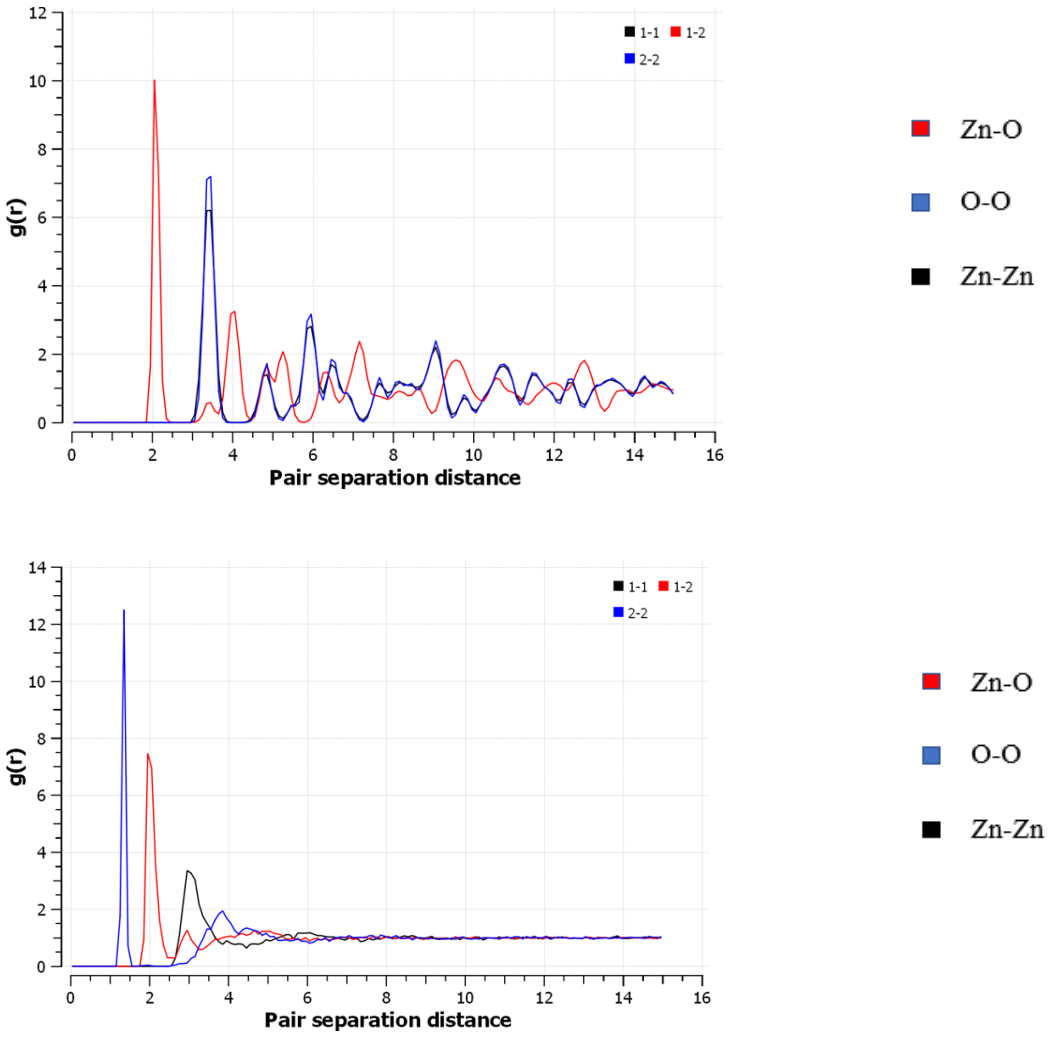

Fig 3.3: RDF of c-ZnO (top) and a-ZnO(bottom). 1- Zn , 2- O (generated with OVITO)

Using the same technique above, the system is further annealed from 300 K to 5000 K and then quenched to 300 K with the same cooling rate (Fig 3.4). However this time the system was not stable at 300 K and the number of defects increased (~818 interstitials and vacancies). From the RDF, probability of finding a bonding atom pair also decresed further (Fig 3.5).

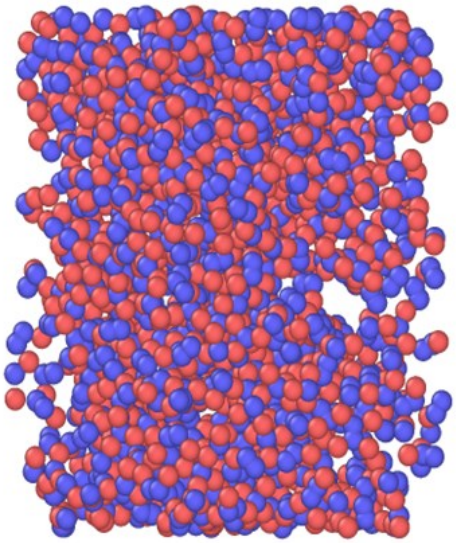

Fig 3.4: Bulk ZnO at 300K after annealing from 2500K in a cooling rate of 100K/ps

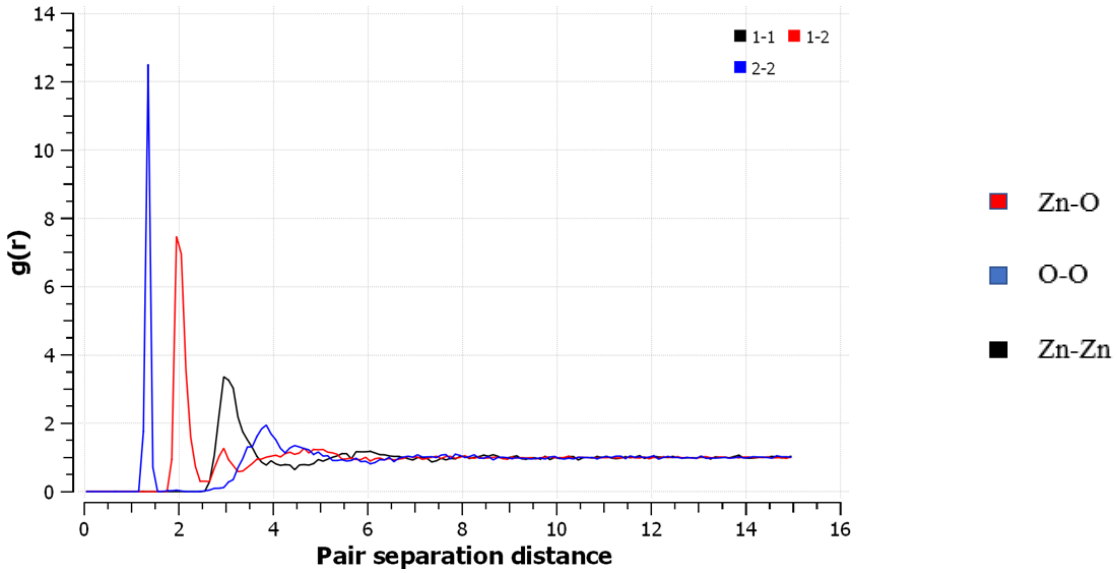

Fig 3.5: RDF of ZnO annealed from 5000 K to 300 K. 1- Zn , 2- O (generated with OVITO)

Laser Irradiation on Al Doped ZnO

We started our experiment with an ALD grown Al:ZnO thin film on Si. The sample was developed at Air force research laboratory (AFRL), USA and was used to understand the nature of annealing effect due to laser irradiation. The crystallinity of the sample was determined from the XRD pattern (Fig 3.6). The peak at 29^0 confirms about the substrate being Si(111) and the main diffraction peak of ZnO appears at $2\theta = 35^0$, which corresponds to the (0002) plane. The XRD result indicates that a wurtzite structure with (0002) orientation (0002) or c-axis growth formed[19].

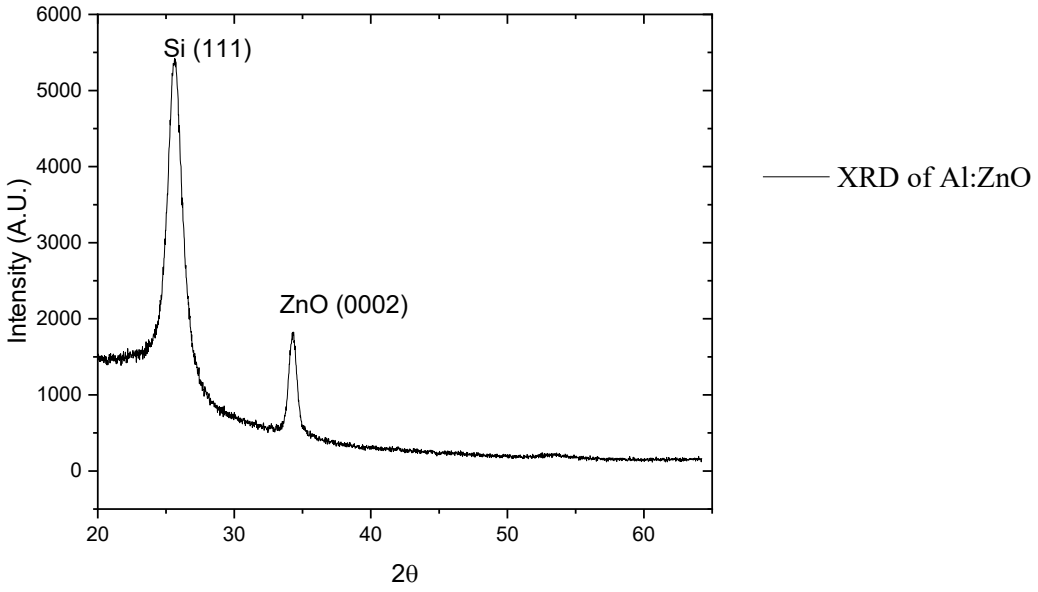

Fig 3.6: X-ray diffraction pattern of Al:ZnO

Photoluminescence (PL) Analysis. Measuring the PL can give information about the deep and shallow energy levels. According to Shalish *et al.,* The deep level emission arises mainly from surface layer, and on the other hand Chang et al., suggests that it arises from the

bulk. Considering the contrast in the argument it can be inferred that the issue is the penetration depth of the excitation light, where the defect states vary with depth[20].

The PL spectroscopy was done with a Horiba LabRam HR800 instrument consisting of a dark chamber to place the sample and an UV-excitation Laser source. The thickness of the sample was approximately 30nm, so this would only cast an absorption of ~50% of the excitation light for a shorter wavelength (~265 nm). Therefore, the laser excitation wavelength was selected at a longer wavelength (325nm). High intensity of the excitation light was achieved by a 15x-NUV objective lens, so that the emission from the bulk of the sample is possible. PL measurement was taken in room temperature by selecting the wavelength range from 350nm-700nm (Fig 3.7).

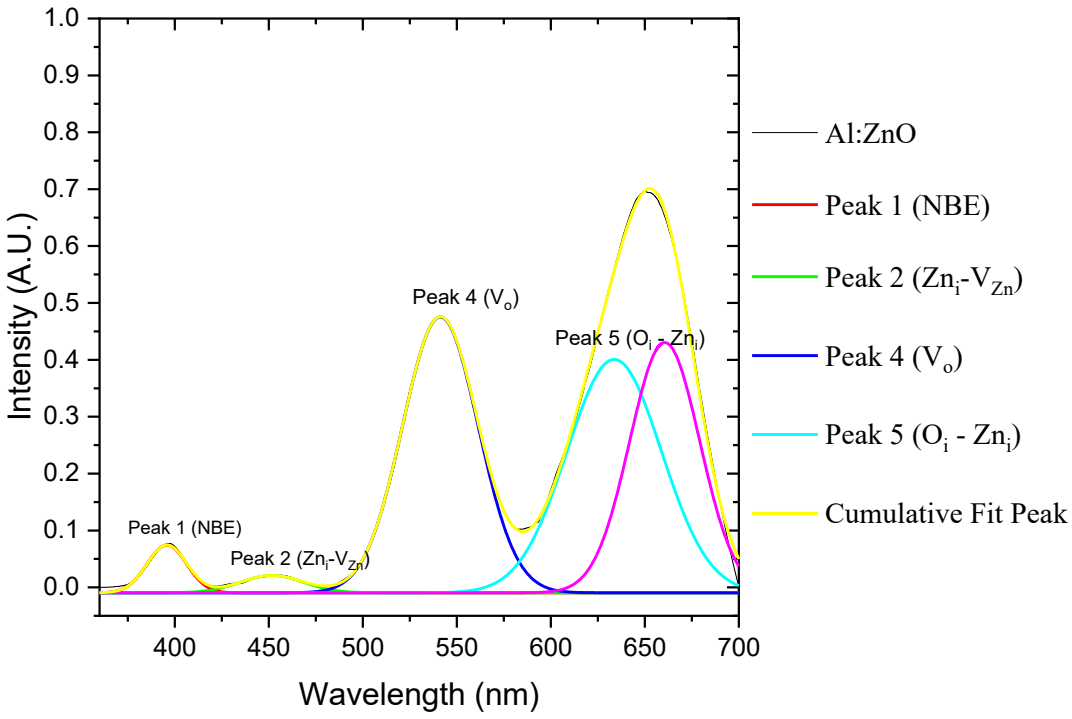

Fig 3.7: PL spectra of Al doped ZnO. Peaks at different wavelengths indicates the emissions due to vacancies and interstitials.

The PL spectra of the Al:ZnO exhibited multiple broad peaks at near 400, 450, 550 and 650 nm Fitting the data with Origin gave five different peaks at 396, 451, 541, 633 and 660 nm. The spectral emission can be attributed as a near band-edge (396 nm), violet-blue (451 nm), and green-yellow emissions, as shown in the PL spectra (541 nm). At room temperature, the peak of NBE emission is usually about 380 nm. However, the cause for the substantially redshifted NBE emission peak (396 nm) could be owing to the competition of emissions at different energy levels. All the emission in the films can be traced back to native defect states. The peak at 451 nm was caused by recombination of Zn interstitial (Zn_i) with Zn vacancies (V_{Zn}). The peak at 541 nm was caused by +2 charged Oxygen vacancies (V_o). In the PL spectra, the intensity of NBE emission is lower than the Deep level emission, which suggest that the film has higher density of surface defects, which also supports the red shift of UV emission in the spectra[21].

The same Q-switched solid state laser source that was used for deposition, was used again for annealing. Considering High laser energy will cause significant ablation on the surface of the film, the energy/pulse was controlled by changing the laser parameters. The source laser wavelength was fixed at 256 nm, The frequency was reduced to 1Hz. The focusing lens was removed to decrease the Energy density. The Pulse width of the laser was kept at 10ns. With these parameters, the energy can be controlled by varying Q-switch delay.

The film was rinsed with Acetone first and then with Ethanol and Distilled Water. A sample holder was placed in front of the laser source. Before placing the film onto the sample holder, a piece of thermal printing paper was attached to the holder. This was done to find out the hitting position of the laser in the sample holder. A circular spot was created on the paper after hitting with the laser. Now the sample could be attached to sample holder in that spot and in this way the film can interact with the laser directly (Fig 3.8).

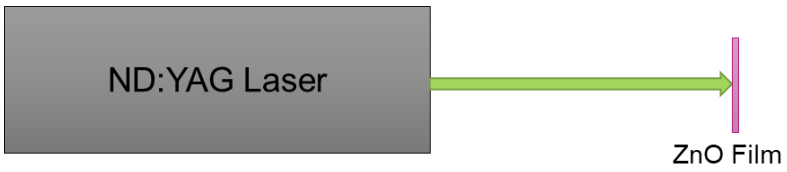

Fig 3.8: The experimental setup for pulsed laser annealing

At first, one laser shot of energy 50 mJ was casted into the sample for annealing. The PL was done just after annealing event (Fig 3.9).

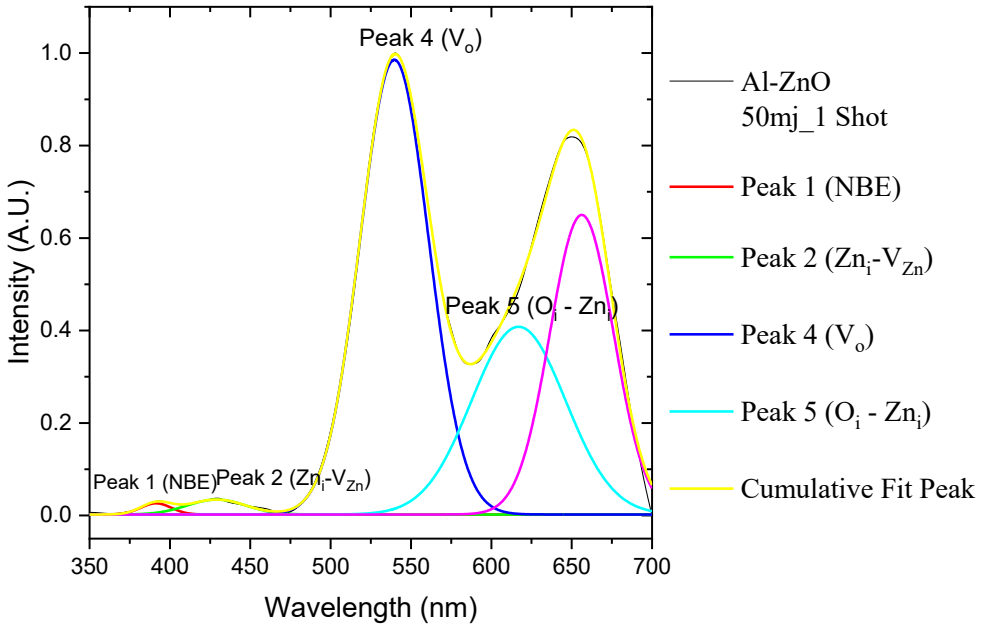

Fig 3.9: PL spectroscopy of Al:ZnO after annealed with one laser shot of 50 mJ energy.

The PL spectra of the Annealed Al:ZnO also exhibited multiple broad peaks at near 400, 450, 550 and 650 nm. Fitting the data with Origin gave all the five different peaks at near the wavelength as of the original sample, with exception of NBE emission peak. The cause for the

slightly blue shifted NBE emission peak (391 nm) can be the attributed as the decrease of the number of different energy levels. But the intensity of the peak also decreased and simultaneously, the peak intensity at 541 nm due to +2 charged Oxygen vacancies (V_o) increased. The peak at 616 nm can be attributed to the recombination of Zn Interstitials (Zn_i) with Oxygen interstitials (O_i). This data suggest that the surface defects of the annealed sample have higher density than the original one, which is contrary to our expectation.

Due to hitting the sample with laser, not any significant surface ablation was observed, which was further verified by the SEM/EDX spectroscopy (3.10-11).

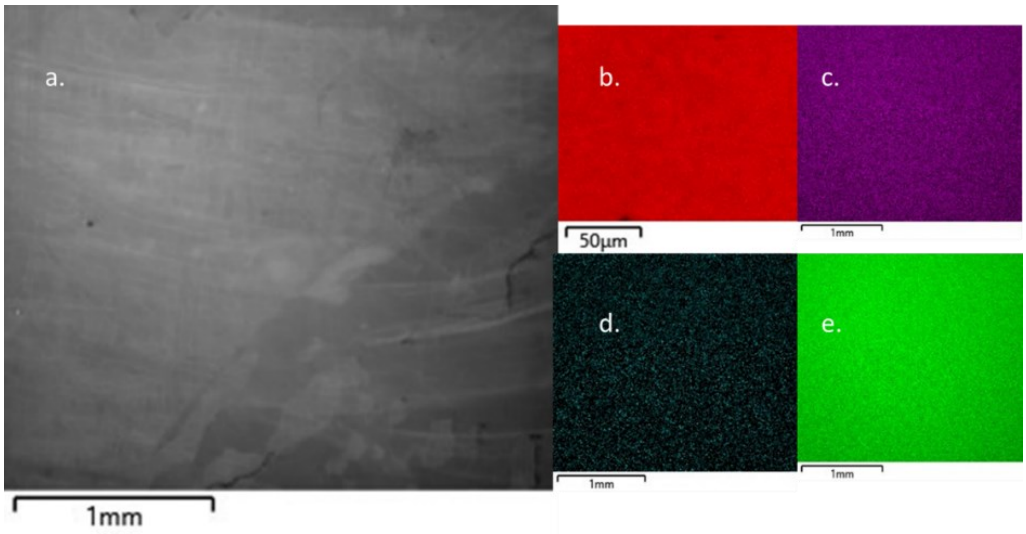

Fig 3.10: a)The SEM image shows no major morphological change due to annealing. EDX image of b) O atom (c) Zn atom, (d) Al atom, (e) Si atom

There is no change in the Raman spectroscopy and XRD pattern after annealing (Fig 3.12). A peak shift in Raman spectra indicates a chemical/physical change, which is not our case[22]. So, crystallinity is intact after annealing.

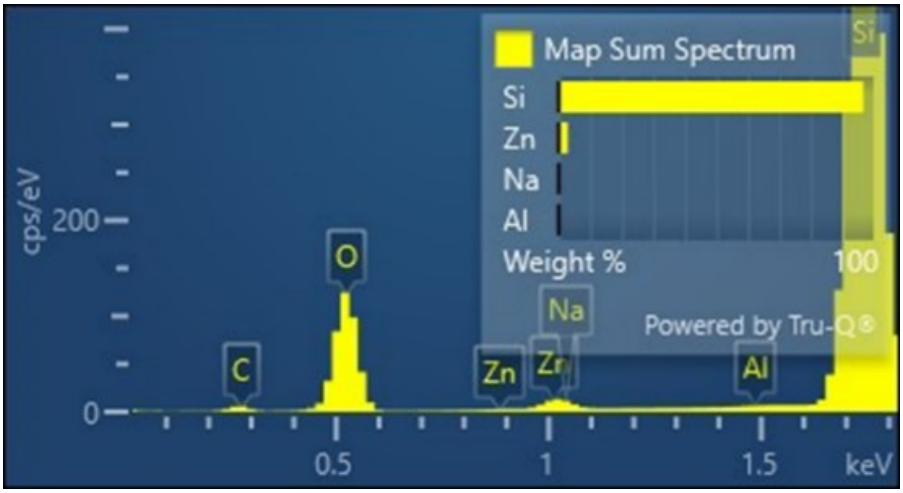

Fig 3.11: The energy dispersive spectra of the sample obtained from the SEM-EDS analysis shows that the sample has pure ZnO phases.

Another Sample of Al:ZnO thin film was taken and this time it was annealed with 50 laser shots with decreased energy of 10 mJ/pulse. After the annealing, the surface ablation was visible in the naked eye and was further analyzed with SEM/EDX spectroscopy (Fig 3.13).

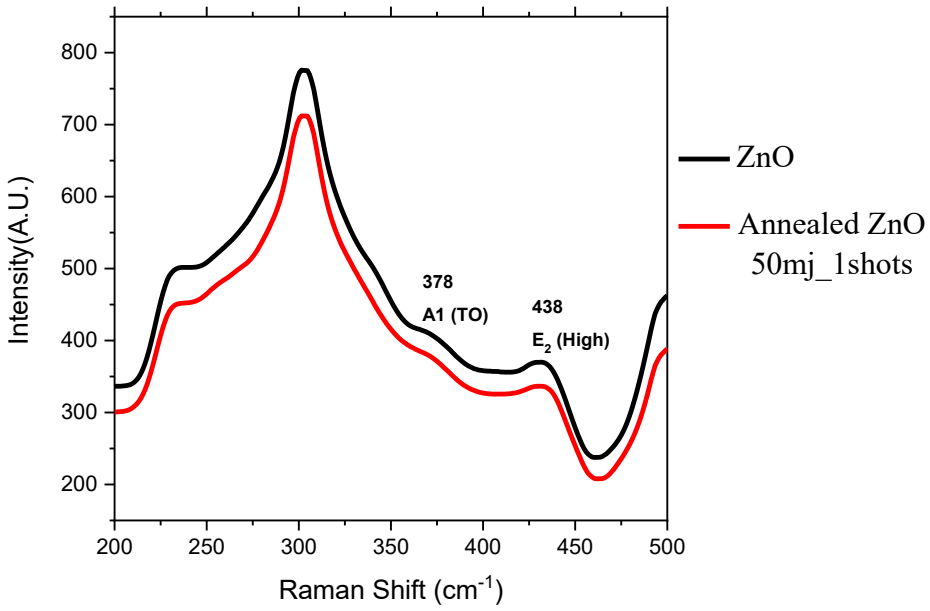

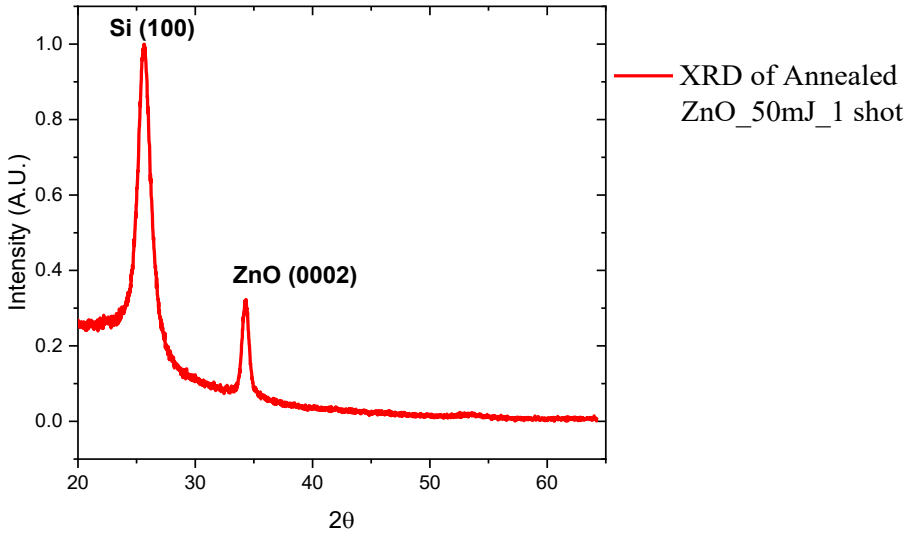

Fig 3.12: Raman spectroscopy of Al:ZnO before and after annealing (top). XRD pattern also didn't change after annealing (bottom).

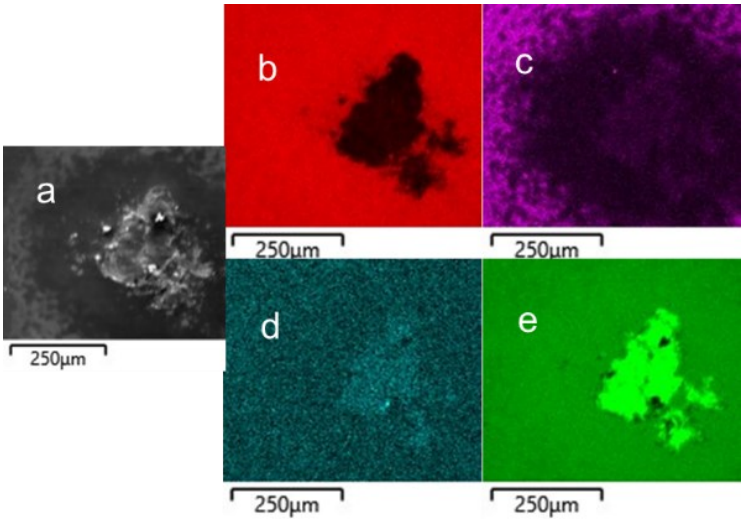

Fig 3.13: a)The SEM image shows significant surface ablation after irradiation. EDX image of b) O atom (c) Zn atom, (d) Al atom, (e) Si atom

The PL spectra of this sample this time gave some interesting data, which showed different multiple broad peaks at near 450, 500 and 600 nm and the peak due to NBE at 360 nm is missing (Fig 3.14). Fitting the data with Origin gave all the four different peaks at 445 nm, 510 nm, 588 nm, 676 nm. The cause for the missing of NBE emission peak (391 nm) can be the attributed as increase of defects in the surface level. It can be also seen from the graph that +2 charged oxygen vacancies (V_o) at 541 nm vanished. But the defects should be increasing due to the missing NBE peak. The 510 nm peak gives us hint about the presence of single charged oxygen vacancies (V_o^+), which was not prominent before. Also, the area under the peak at 445 nm increases and the recombination peak at ~600 slightly blue shifted to 588 nm, which means the number of energy levels decreased but the area under the peak increased (Table 1) which suggest that this energy level has higher density of deep level defects. Combing all these factors, it can be concluded that both surface level and deep level defects has been increased due to annealing.

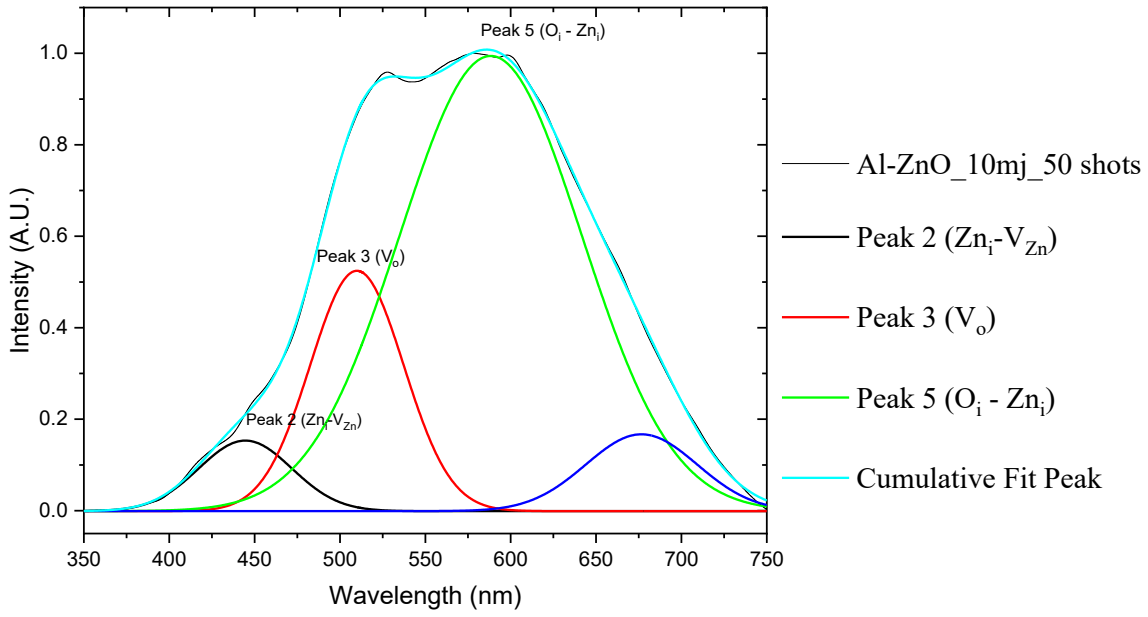

Fig 3.14: PL spectroscopy of Al:ZnO after annealed with 50 laser shots of 10 mJ energy.

Table 1: Area under the peaks for different annealing parameters.

Sample	Peak 1 (~390 nm)	Peak 2 (~440 nm)	Peak 3 (~500 nm)	Peak 3 (~540 nm)	Peak 5 (~602 nm)
Al:ZnO	2.2	1.3	----	24.38	25.84
Al:ZnO_50mj_1 shot	0.57	1.47	----	52.51	29.77
Al:ZnO_10mj_50 shots	-----	10.52	36.11	----	132.9

Overall, it can be inferred from the above experiment that the native point defects inside ZnO thin films can be modified using pulsed laser annealing. Though for the above parameters we used in our experiments, we couldn't reach our goal which is to decrease the level of defects. And in the second case, the surface endured a significant amount of damage due to laser irradiation. To minimize the ablation at the surface level, we need to increase heat penetration depth. The sample we used for this experiment was ~30nm thick, so we need a thicker sample for a balanced distribution of heat while irradiaing with Laser. And a suitable combination of Laser Energy and Number of shots is needed to modify the defects to the desired point.

PLA with PLD Grown ZnO Thin Films (Sample 1)

The first sample we grow with PLD was ZnO thin film on Si substrate. Due to maintaining long deposition time and large number of laser shots, the film was thick enough for proper laser pulse heating. The film was grown on 400^0C, so a large number of defects can be anticipated from the PL spectroscopy. At first PL measurement was taken to identify the defects of the ZnO film (Fig 3.15).

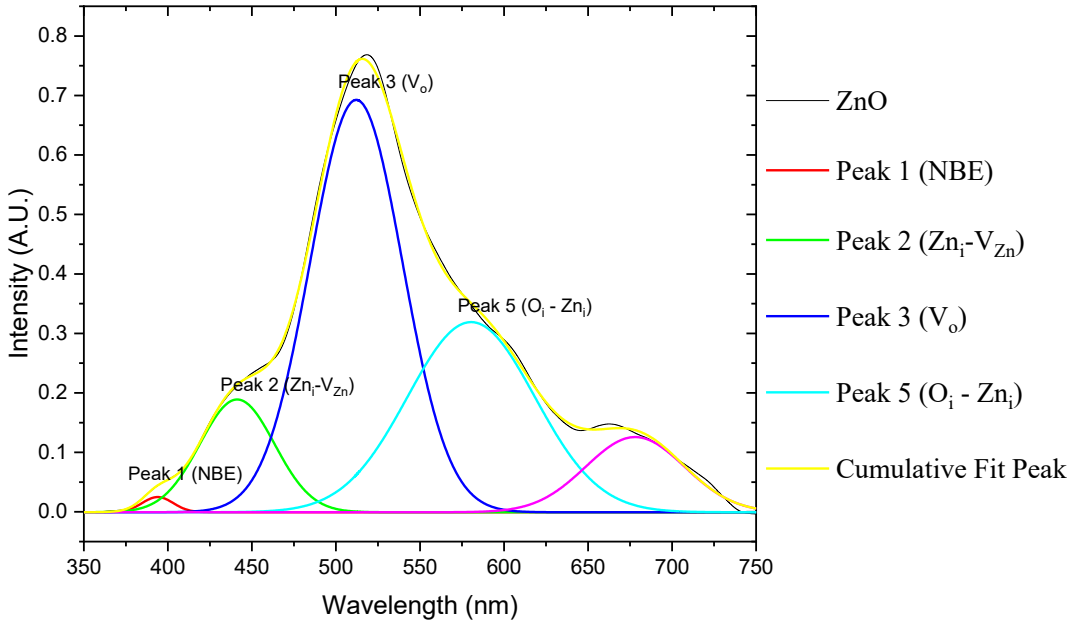

Fig 3.15: PL spectra of ZnO/Si thin film grown with PLD at temperature 400^0C and O_2 pressure of $1.9x10^{-2}$ mbar

PL spectra of the sample exhibited multiple broad peaks at near 400, 450, 500 and 600 nm. Fitting the data with Origin gave five different peaks at 394, 441, 512, 580 and 678 nm. The substantial redshift of NBE emission peak (394 nm) can be attributed to the competition of emissions at different energy levels like before. All of the emissions in the films can be traced back to native defect states. The peak at 441 nm was caused by recombination of Zn interstitial (Zn_i) with Zn vacancies (V_{Zn}). The interpretation about the peak at 512nm was caused by either +2 charged or single charged Oxygen vacancies (Vo). Generally Single charged V_o peaks are found near 510 nm, however as the V_o^+ has high formation enthalpy, it is possible that V_o^{2+} vacancies had a significant blue shift due to emission from limited number of different energy levels. We will know more about it further after annealing is done. The peak at 580 nm can be attributed to the recombination of Zn Interstitials (Zn_i) with oxygen interstitials (O_i). In the PL spectra, the intensity of NBE emission is significantly lower than the Deep level emission, which

suggest that the film has higher density of surface defects, which also supports the red shift of UV emission in the spectra.

The PLA was carried out with the previous setup. Considering the surface ablation and the results from the previous experiments, it was decided to keep the laser pulse energy under 20 mJ and number of shots was varied from 1 to 10 by keeping the Laser frequency same as before (1 Hz). The procedure represented as a matrix from is shown on Fig 3.16.

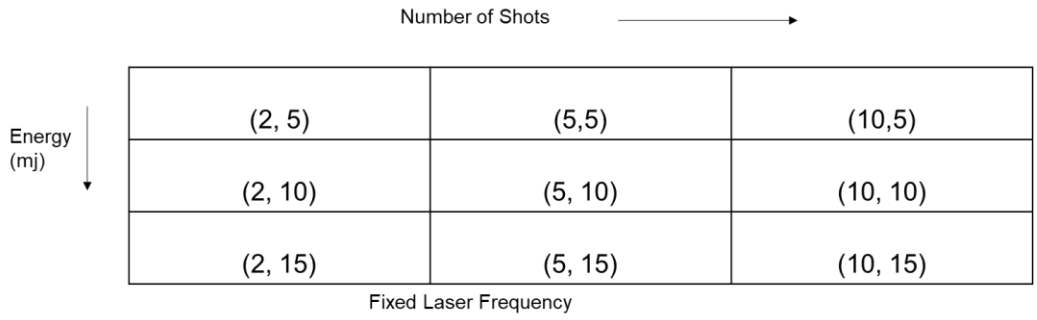

Fig 3.16: Combination of variable laser energy and number of shots in matrix form

The Pulsed Laser Annealing was carried out following the parameters from Fig 3.16. But with the parameters, not any significant change was observed in the PL Spectroscopy. The reason could be the increased thickness of the film and insufficient laser energy to cast a significant change in the surface level. Frequency of the Laser Pulse shot could also play a significant role, as after one Laser pulse was provided, because of the high diffusion rate of the atoms the structure regained its previous state before interacting with the next Laser Pulse.

The workflow that was followed to find out the suitable parameters have been presented with the help of a flowchart below (Fig 3.17).

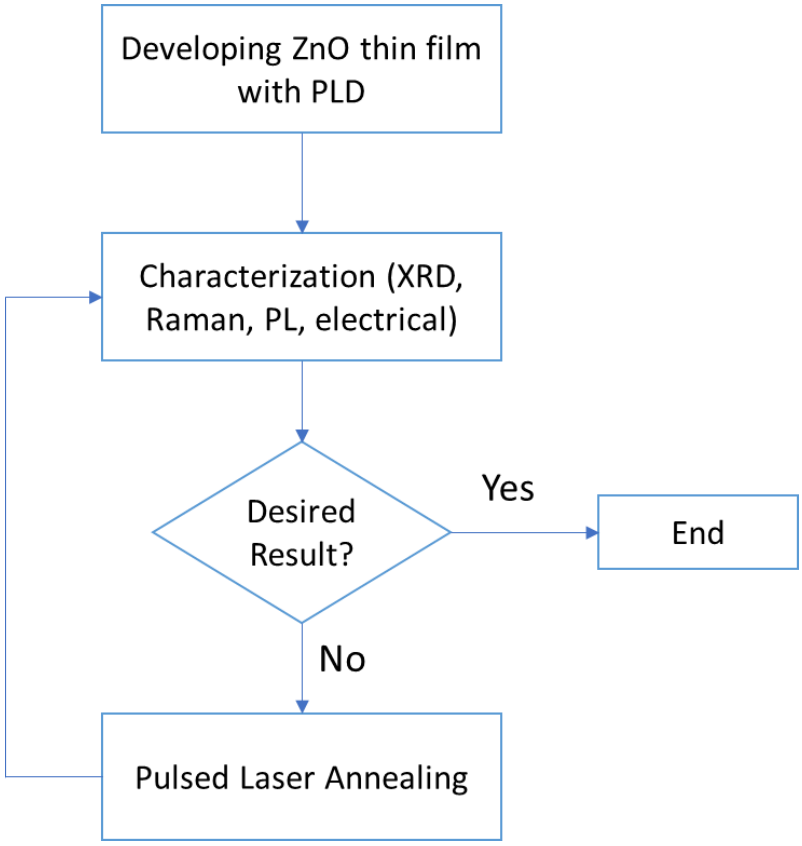

Fig 3.17: Flowchart of the experimental work

So, in the next step the experiment was carried out with an increased laser frequency (2 Hz), The energy of the Laser Pulse was kept between 15-20 mJ/pulse and total 10 shots were provided. After annealing was done, the sample was placed in the Horiba LabRam HR800 chamber for doing PL spectroscopy. The sample holder in the chamber can be moved in the x,y,z direction. Inside the chamber with a help of a light source the sample can be also illuminated with a visible light so that the movement can be understood. The movement in 'z' direction is mainly done for focusing, so moving the sample in the x,y direction can provide the image of the whole film surface and it's possible to do the optical spectroscopy mapping. While the annealed sample was analyzed with the visible light emission by focusing with 15x-NUV lens, an interesting portion of the surface area was found (Fig 3.18).

The middle portion of the film provided a Violet-Green emission in the visible range, while the surrounding area provided green emission which is the defect enriched region. The approximate diameter of the portion can be estimated as 2 µm. PL measurement at this portion gave the desired result, all the green emissions ware minimized.

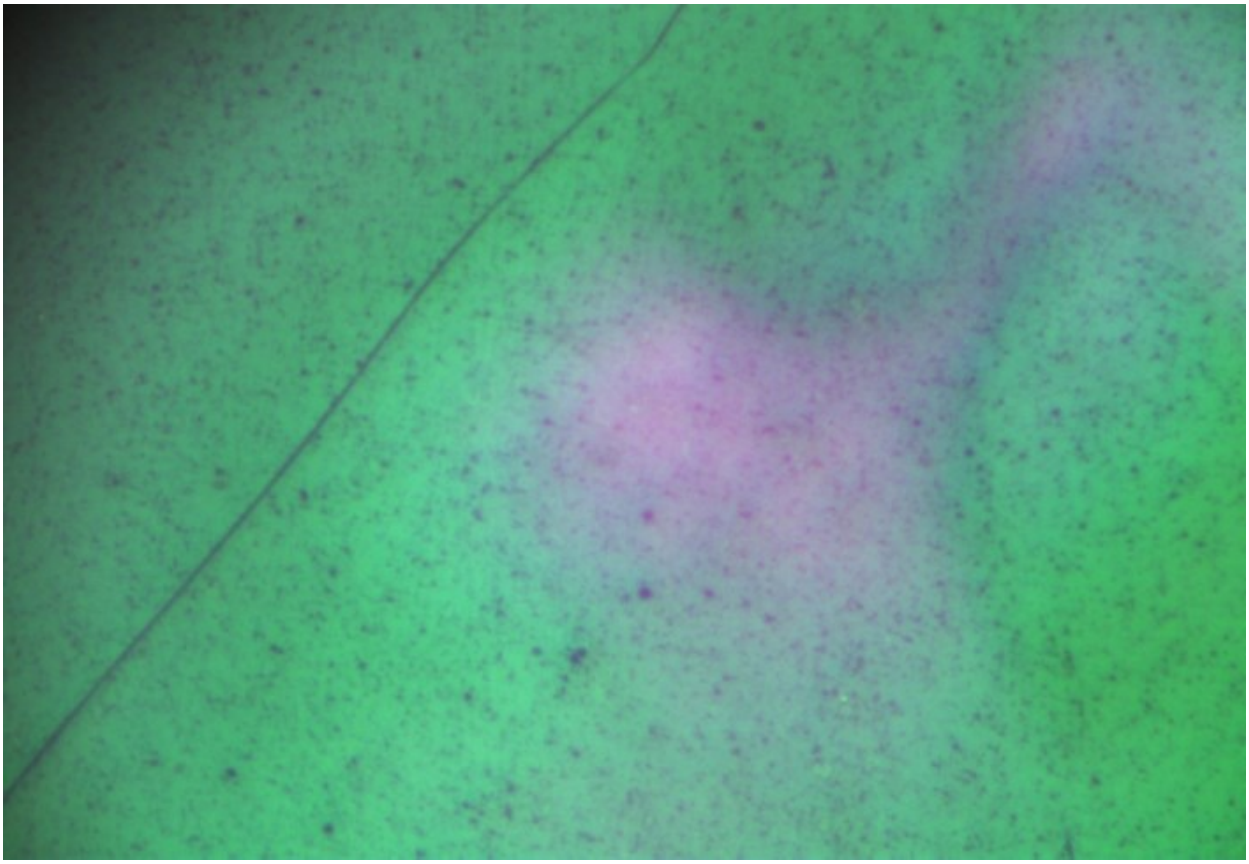

Fig 3.18: Image of annealed ZnO film from the Horiba LabRam HR800 [5 µm]

Fitting the PL data with Origin gave four different peaks at 384, 463, 560 and 756 nm (Fig 3.19). The substantial blueshift of NBE emission peak (384 nm) clearly indicates that competition of emissions at different energy levels have decreased because of the stability of the structure. The peak at 463 nm which was caused by recombination of Zn interstitial (Zn_i) with

Zn vacancies (V_{Zn}) has been removed. Zn interstitials are shallow donors and their transition to acceptor level created the vacancies and gives rise to PL around 440 nm. From the missing peaks it can be inferred that the Zn interstitials diffused into crystal and the open volume which created the Zn vacancies were filled. As a result, the defect from the Zn sites were removed. In the same process, the oxygen interstitials diffused into the crystal and filled the oxygen vacancies (V_o). A small amount of oxygen vacancies was observed at 560nm, which decreased significantly after annealing. The peak at 756 nm can be attributed to the doublet of UV emission at 384nm. In the PL spectra, the intensity of NBE emission is significantly higher than the deep level emission, which suggest that the film has lower density of surface defects, which also supports the blue shift of UV emission in the spectra.

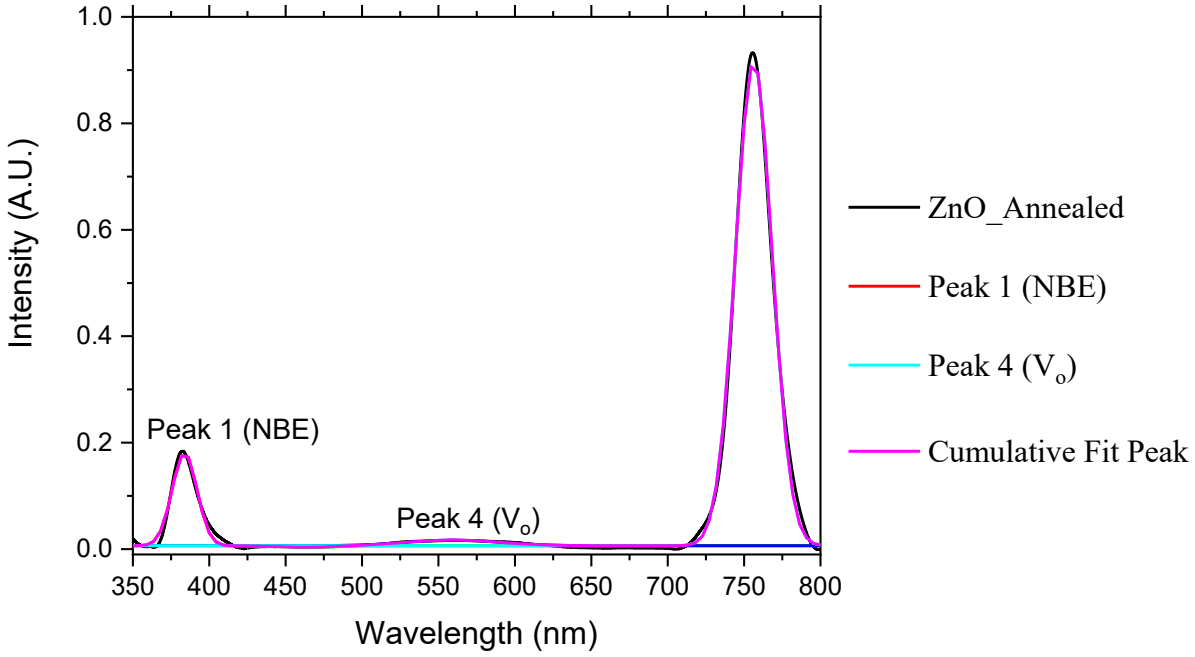

Fig 3.19: PL spectroscopy at the 1st spot of the annealed film

Considering the result above, a PL mapping was done for the whole sample and measurement was taken from another seven spots (Fig 3.20-24). For most of the spots significant blueshift of NBE emission was observed and the intensity of the peaks from the defects was decreased. The change in the area under the peaks are given in Table 2.

From the PL spectra of Fig 3.20, both the Single and +2 charged oxygen vacancies are present, which is evident from the peaks at 514 and 563 nm. This data also verifies the presence of only single charged V_o in the original sample and due to annealing, energy level of some of the single charged vacancies shifted from near the conduction minimum to near the valence band maximum and became +2 charged V_o. Fewer Zn interstitials are there in the sample and it recombines with few Oxygen interstitials hence gives rise to the peak at 600 nm[23]. The NBE emission is also blue shifted at 385 nm so there are fewer surface defects than the original sample.

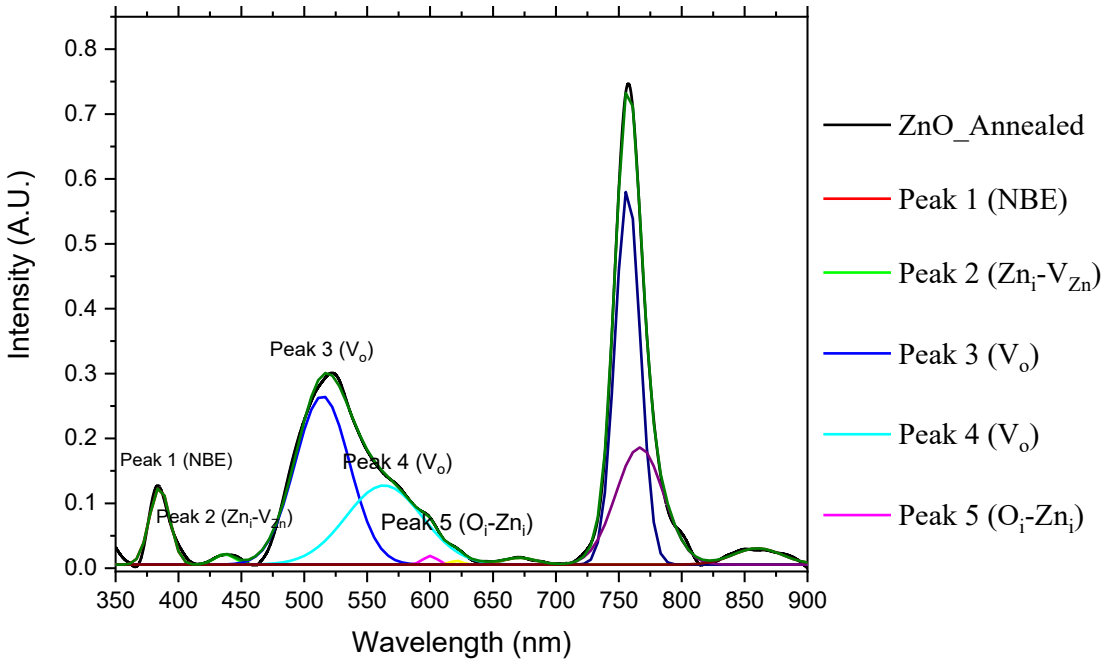

Fig 3.20: PL spectroscopy at the 2nd spot of the annealed film

For the third spot (Fig 3.21), the peaks at 531 and 590 nm indicates showed significant decrease in the defect levels. Though the NBE emission peak at 392 nm increased, which is confirmed by the red emission doublet at 695 nm, the red shift indicates there are still different number of energy bands available at this range.

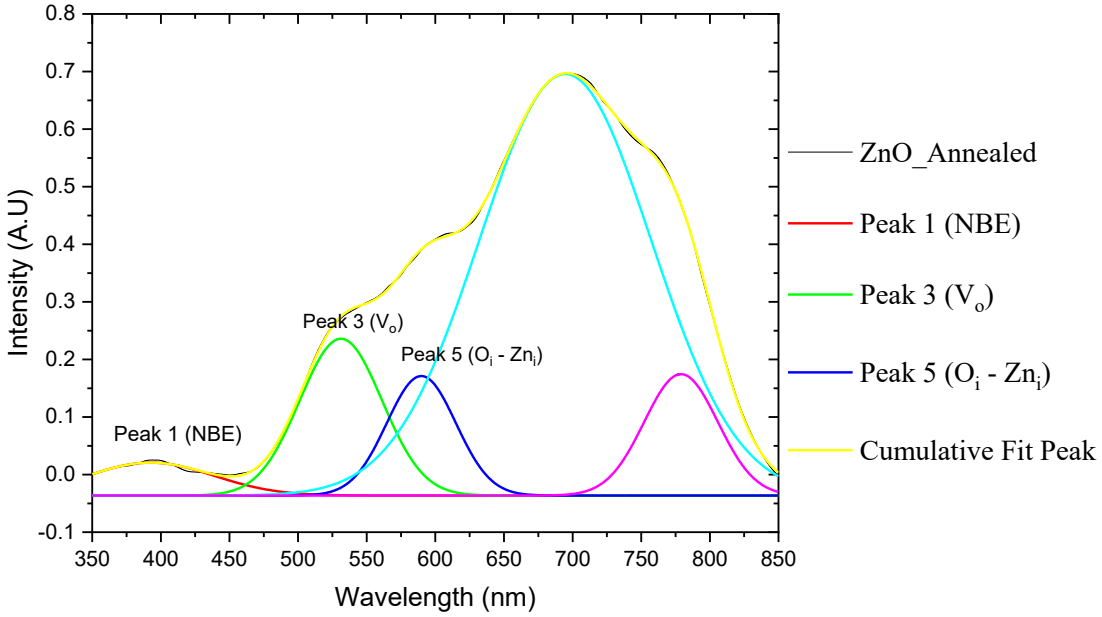

Fig 3.21: PL spectroscopy at the 3rd spot of the annealed film

PL spectra at 4th and 5th spot also gave us the same interpretation from the 3rd spot (Fig: 3.22). PL spectra of 6th and 7th spot didn't show any significant change due to annealing (Fig 3.23). The intensity of the NBE Emission peak near 390nm decreased and introduced more deep level defects. The PL spectra of the 8th spot (Fig 3.24) of the annealed film is almost similar to the spectra of the 2nd spot where NBE emission is blue shifted and the single charged V_o converted to +2 charged V_o. In the table 2, the area under the peaks are given and from the data a comparison can be drawn for different spots.

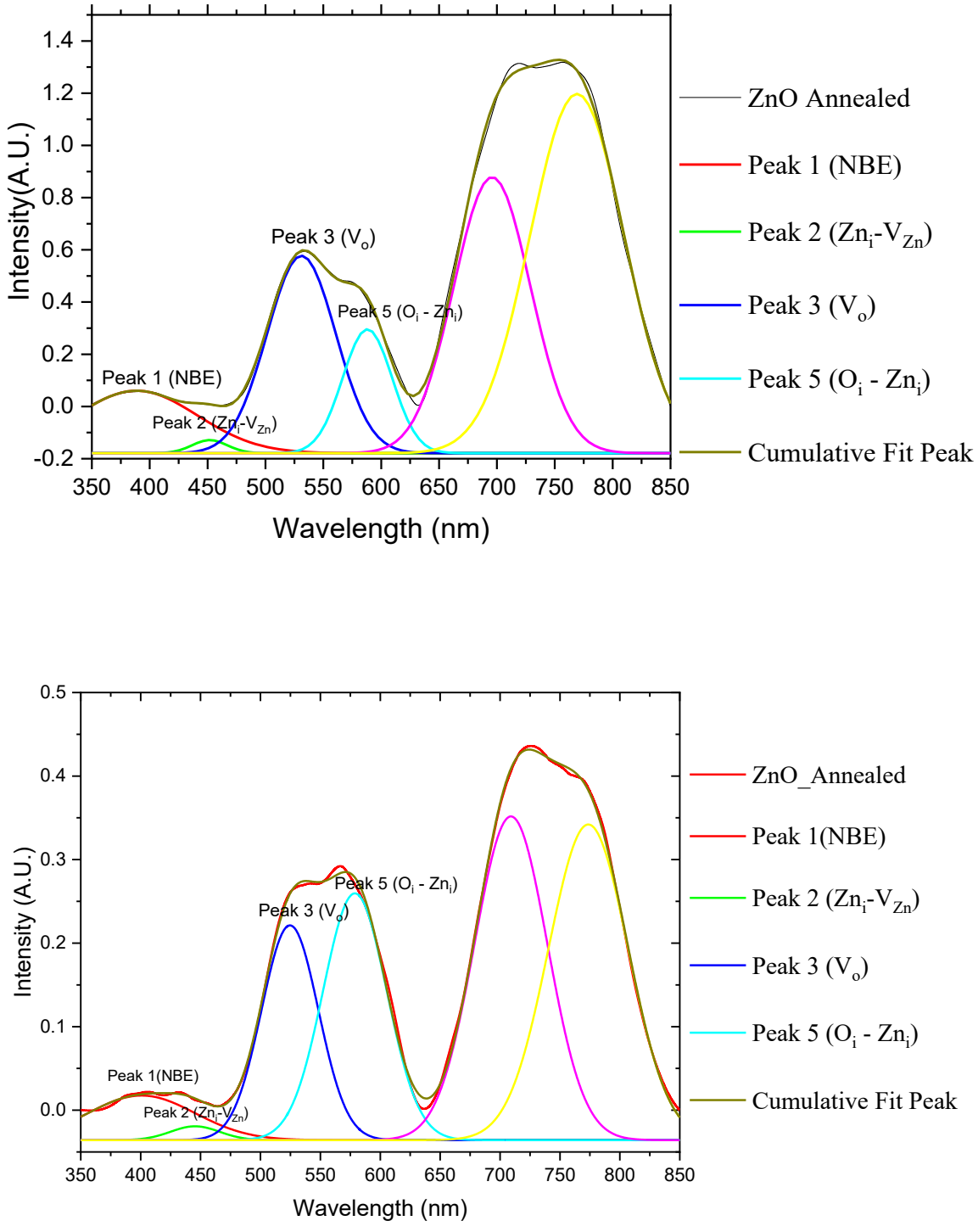

Fig 3.22: PL spectroscopy at the 4th (top)& 5th (bottom)spot of the annealed film

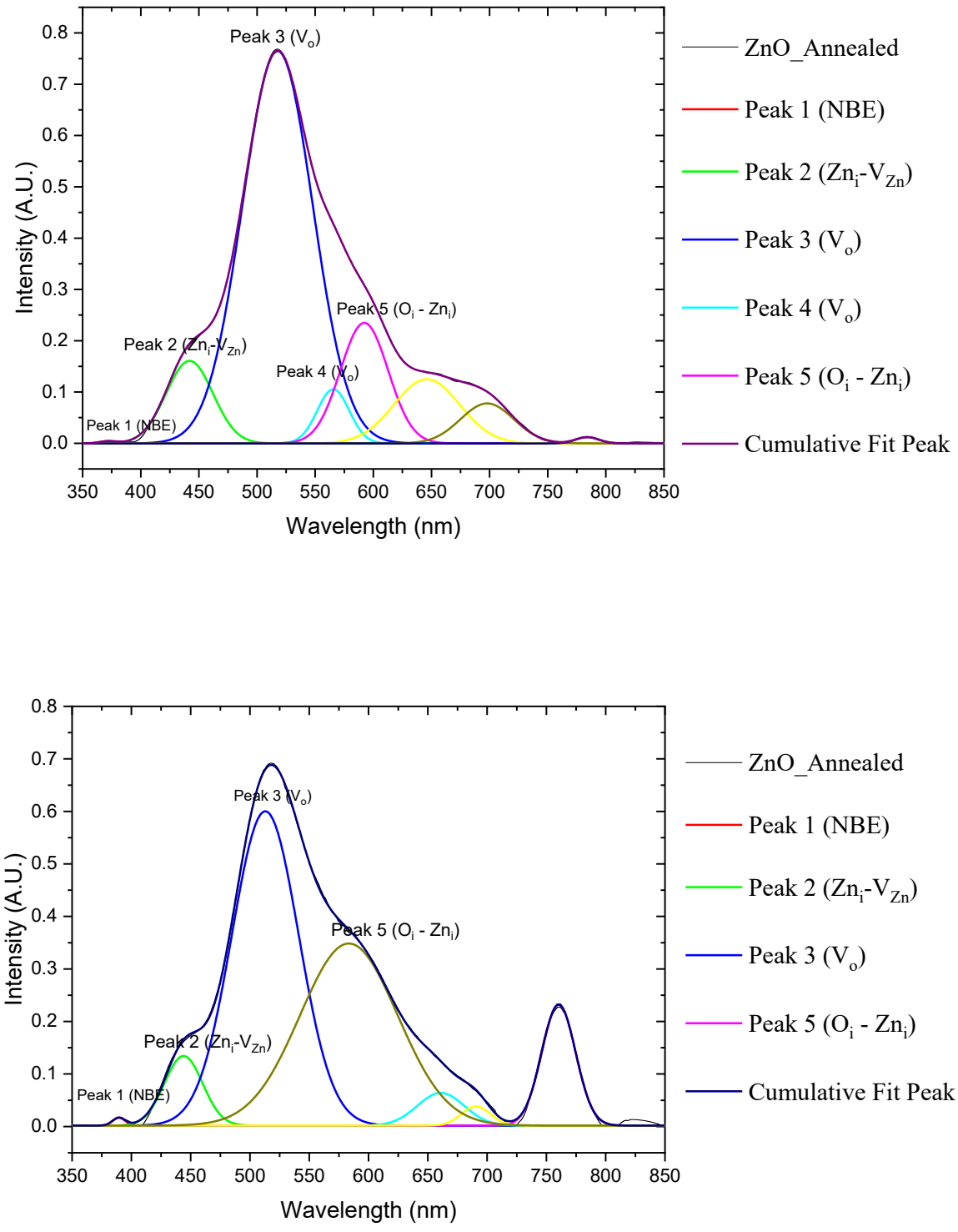

Fig 3.23: PL spectroscopy at the 6th & 7h spot of the annealed film

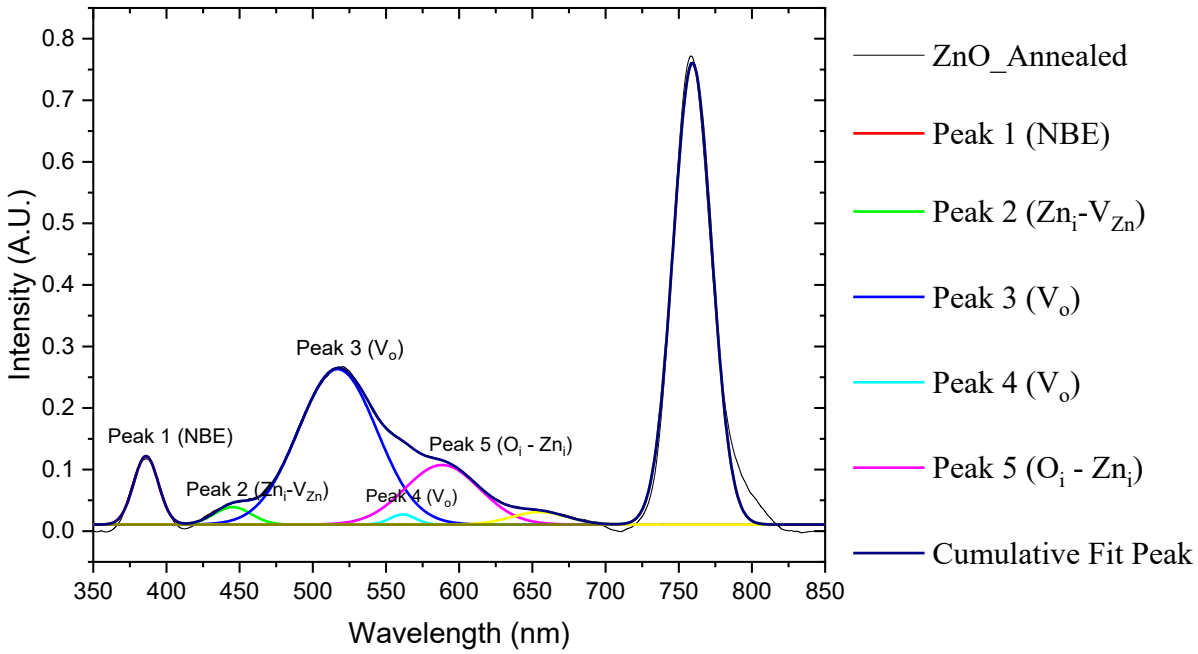

Fig 3.24 : PL spectroscopy at the 8^h spot of the annealed film

Table 2: Area under the peaks for different annealing parameters for ZnO/Si thin film.

Sample	**Peak 1 (~390 nm)**	**Peak 2 (~440 nm)**	**Peak 3 (~500 nm)**	**Peak 3 (~540 nm)**	**Peak 5 (~602 nm)**
ZnO	0.59	10.54	47.75	-----	30.37
Annealed ZnO_Spot 1	3.55	0.15	------	0.81	-------
Annealed ZnO_Spot 2	2.4	0.32	50.77	9.28	0.07
Annealed ZnO_Spot 3	6.58	-----	20.47	-----	13.1
Annealed ZnO_Spot 4	31.5	1.9	56.21	-----	25.48
Annealed ZnO_Spot 5	5.98	0.85	15.3	-----	19.64
Annealed ZnO_Spot 6	0.08	8.1	58.07	3.65	12.1
Annealed ZnO_Spot 7	0.2	5.35	42.3	-----	35.74
Annealed ZnO_Spot 8	2.35	0.9	17.04	0.36	6.18

In this section the most important finding is the suitable Laser parameter for annealing. Though we got the desired result but the whole film itself is not free of defects. Only one spot of 2µm diameter showed promising result and in the other spots, though the number of defects decreased in few places but not removed totally. And in few spots the defect level was almost same as the original. So, the overall quality of the film didn't change significantly. The reason could be the growth parameter of the film while deposited with the vacuum chamber. The film was grown on a substrate temperature of 400^0C with Oxygen pressure of 1.9x10-2 mbar. It is expected that growing the film with an increased temperature and pressure can give a better quality film, thus a better annealing result.

PLA with PLD Grown ZnO Thin Films (Sample 2)

The second sample we grow with PLD was ZnO thin film on SiO_2/Si substrate (Fig 3.25). The reason behind choosing this substrate over Si is that, almost of the electronic devices consists of transistors and growing ZnO on a stacked structure of insulator-semiconductor will give the opportunity to study the aspects of the annealing in thin film transistor level and will allow to study the transistor characteristics. Due to maintaining long deposition time and large number of laser shots, the film was thick enough for proper laser pulse heating. The film was grown on 600^0C, so fewer defects are anticipated from the PL spectroscopy.

Fig 3.25: ZnO thin film grown on a stacked structure of SiO_2/Si, ZnO works as a conducting channel.

The crystallinity of the sample was determined from the XRD pattern (Fig 3.26). The peak at 69^0 confirms about the substrate being Si (400). The peak at 290 confirms about the substrate being Si(111) and the main diffraction peak of ZnO appears at $2\theta = 35^0$, which corresponds to the (0002) plane. The XRD result indicates that a wurtzite structure with (0002) orientation (0002) or c-axis growth formed at substrate temperature 600^0.

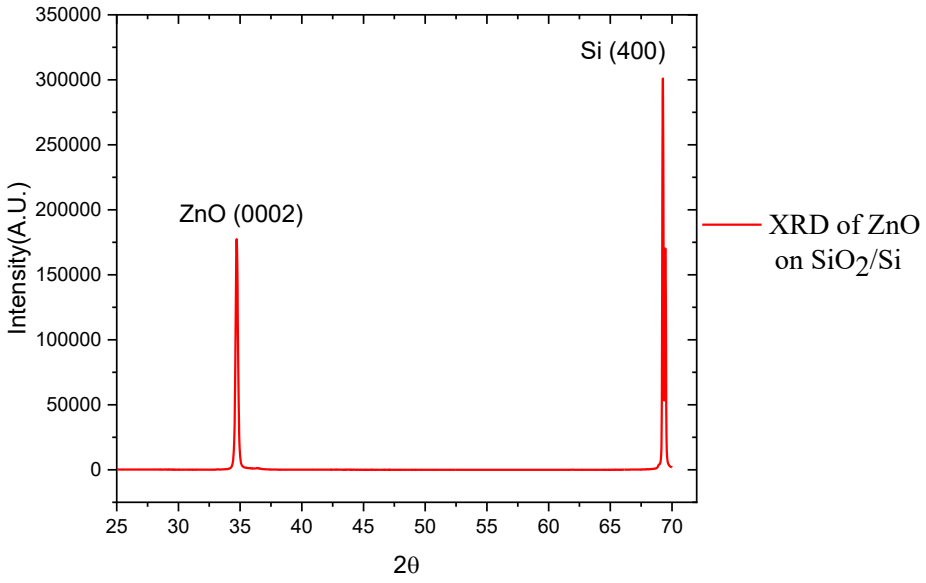

Fig 3.26: X-ray diffraction pattern of ZnO thin film on SiO_2/Si substrate

The Raman spectroscopy (Fig 3.27) showed transverse optical (TO) phonon at 378 cm^{-1}, longitudinal optical (LO) phonon 581 cm^{-1}, and E2 phonons at 101 cm^{-1} (low) and 438 cm^{-1} (high). The electrical characterization was done with a keithley 4200a-scs parameter analyzer. The sample was placed at the CASCADE M150 probe stage and connected to the output line of the probe station with the help of movable contacts. The high-performance parameter analyzer allows current-voltage (I-V), capacitance-voltage (C-V) and ultra-fast pulsed I-V measurements.

I-V characteristics of the sample was measured by connecting the instrument with the probe station, by selecting the voltage range from -1 volt to +1 volt.

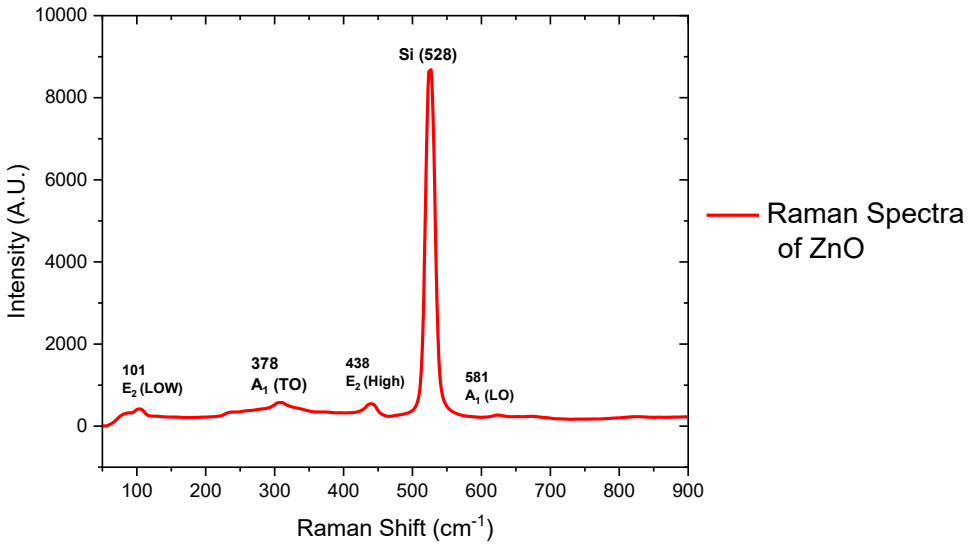

Fig 3.27: Raman Spectroscopy of ZnO thin film on SiO2/Si substrate.

From the I-V characteristics the resistivity was found approximately 4 k-ohm (Fig 3.28). By measuring the spatial parameters, the conductivity can be measured easily (conductivity = 1/resistivity).

The PL spectra of the sample exhibited multiple broad peaks at near 400, 550, 650 and 750 nm. Fitting the data with Origin gave five different peaks at 386, 555, 625, 670 and 770 nm (Fig 3.29). The peaks of the emission in the film can be traced back to native defect states. The peak at 451 nm is missing as the recombination of Zn interstitial (Zni) with Zn vacancies (VZn) is not possible in the absence of Vzn. The peak at 555 nm was caused by +2 charged oxygen vacancies (Vo) and it has lower intensity than the UV emission at 386 nm, which indicates fewer defects. There are also Zn interstitials present in the sample and it recombines with few Oxygen interstitials hence gives rise to the peak at 620 nm. In the PL spectra, the intensity of NBE

emission is higher than the deep level emission, which suggest that the film has fewer surface defects, which also supports the blue shift of UV emission in the spectra. These data suggests that overall quality of the film is better than the sample 1.

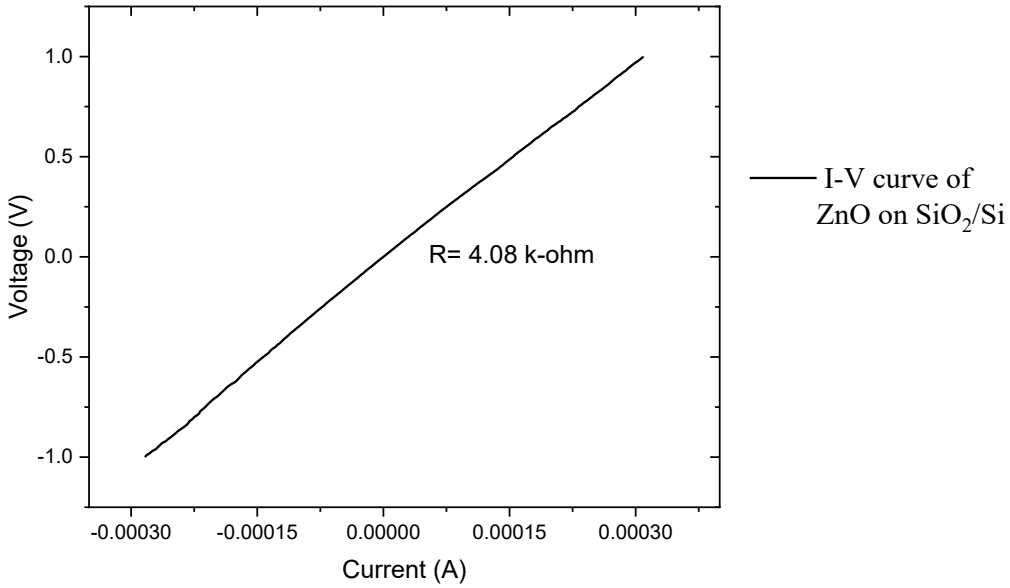

Fig 3.28: I-V characteristics of ZnO

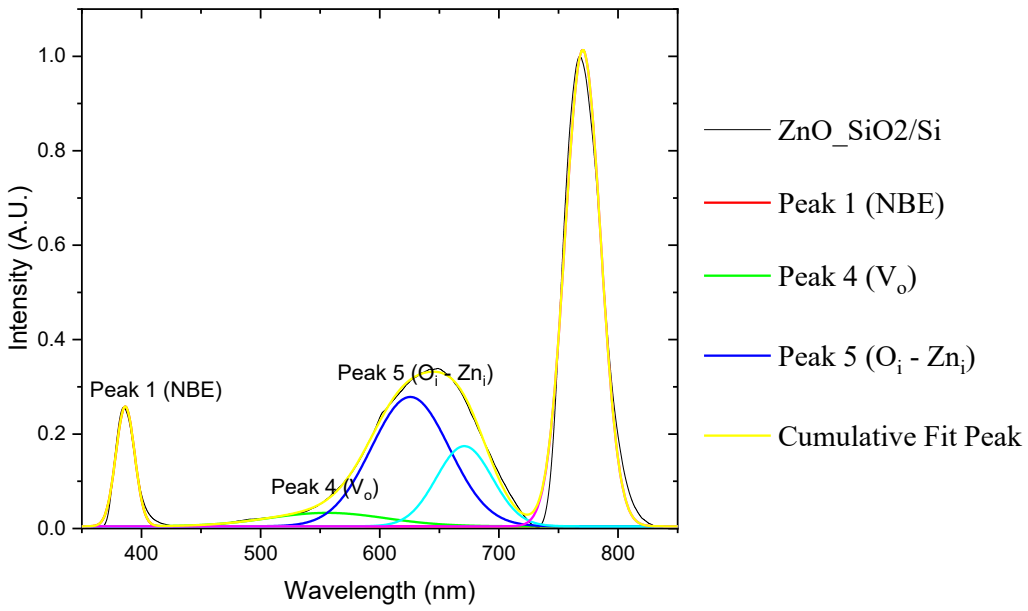

Fig 3.29: PL Spectroscopy of ZnO thin film on SiO2/Si substrate.

For annealing, at first the sample was irradiated with two laser shots. The parameters are same as before (Energy/Pulse ~ 18 mJ, Frequency 2Hz). The I-V characteristics was measured at first, selecting the voltage range from -1 volt to 1 volt (Fig 3.30).

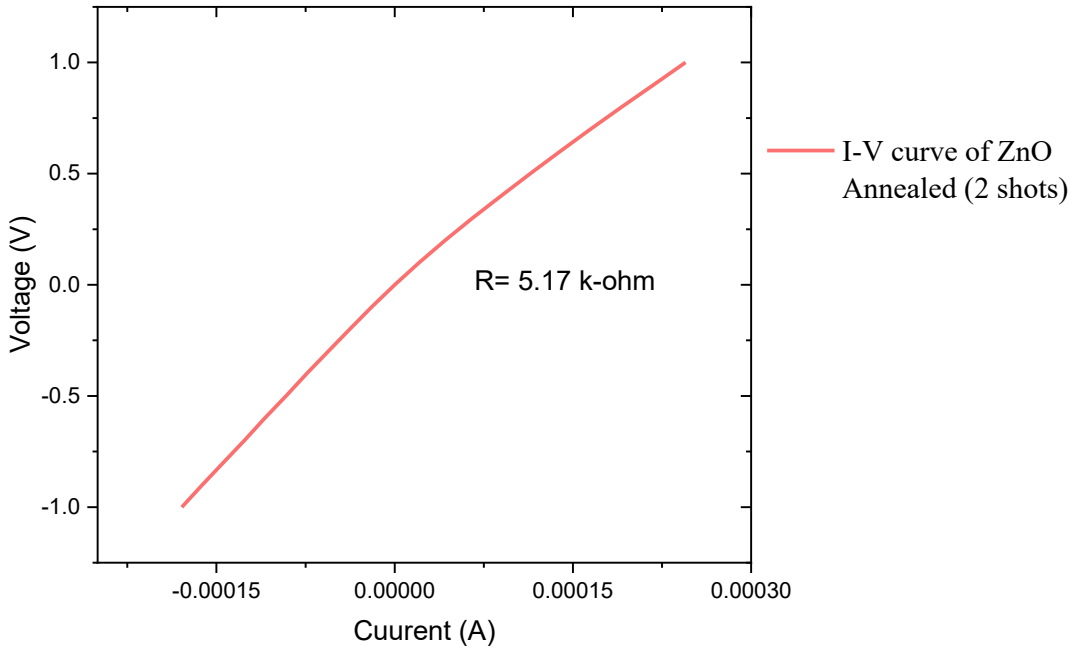

Fig 3.30: I-V characteristics of annealed sample (2 laser shots)

From the I-V measurement, the resistance was found approximately 5.17 k-ohm, which is greater than the original sample. As the resistivity increased, the conductivity also decreased due to annealing. After Giving 5 more Laser shots, The I-V measurement was done again, selecting the voltage range from -1 volt to 1 volt. This time the resistance was found approximately 4.85 k-ohm (Fig 3.31). So, the conductivity increased a little but still lot lower than the original sample. The PL spectroscopy in multiple points was done to determine the defect state of the annealed sample (Fig 3.32)

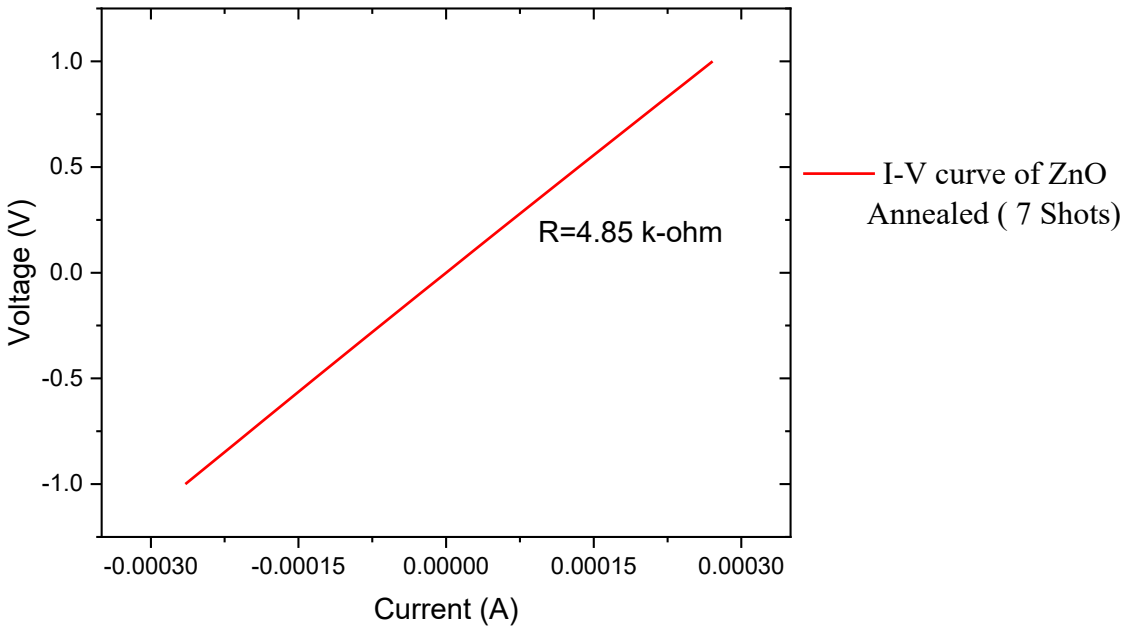

Fig 3.31: I-V characteristics of annealed sample (7 laser shots)

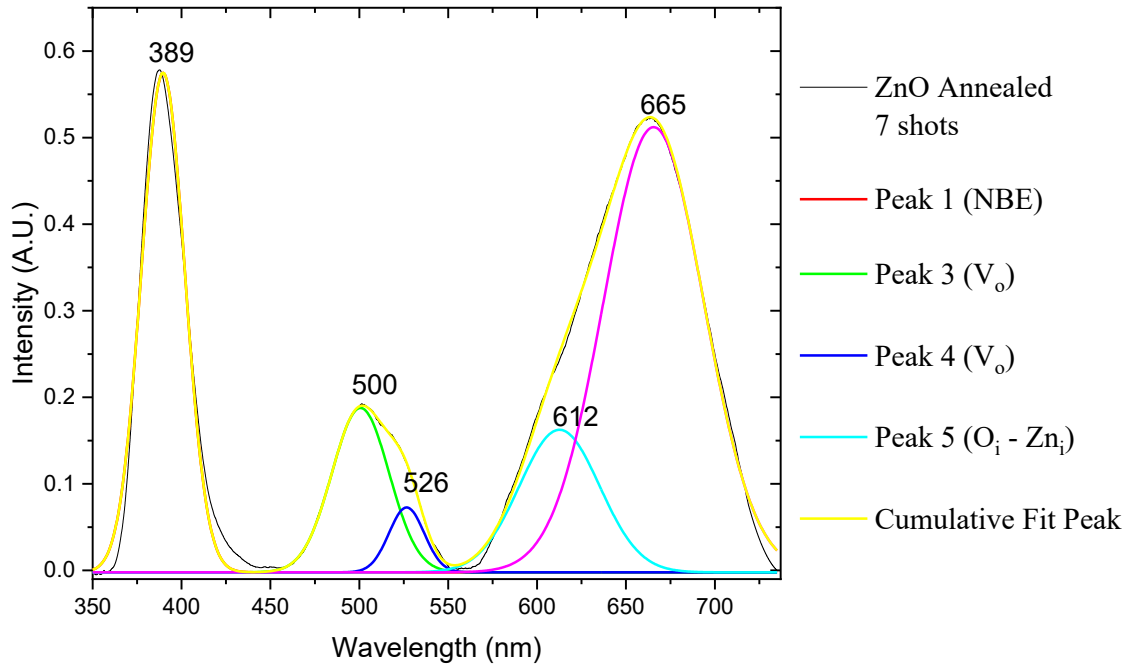

Fig 3.32: PL spectroscopy of annealed ZnO (7 shots)

From the peaks, it is evident that the intensity of the NBE emission at ~390 has been increased. The peak at 451 nm is almost missing as recombination of Zn interstitial (Zni) with Zn vacancies (V_{Zn}) is not possible due to absence of Zn vacancies. The peak near 500 nm was caused by +1 charged Oxygen vacancies (Vo), which was not present in the original sample. The graph also contains +2 charged oxygen vacancy, and the intensity is higher than the original sample. There are also Zn interstitials present in the sample and it recombines with few Oxygen interstitials hence gives rise to the peak at ~610 nm. In the PL spectra, the intensity of NBE emission is higher than the Deep level emission, which suggest that the film has fewer surface defects, But the deep level defects have been increased than the original sample which explains the decrease of the conductivity of the sample.

After giving 3 more laser shots, the I-V characteristics was measured again, selecting the voltage range from -1 volt to 1 volt (Fig 3.33).

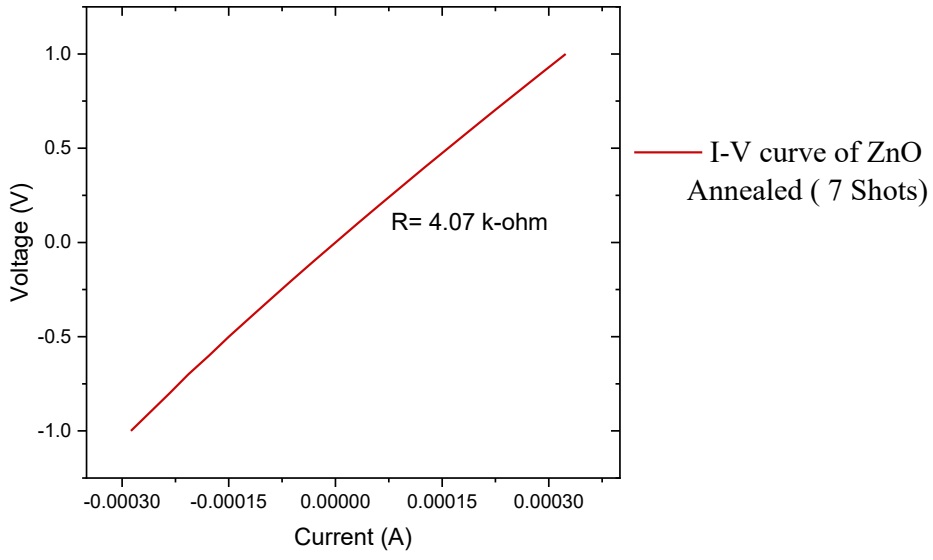

Fig 3.33: I-V characteristics of annealed sample (7 laser shots)

This time the resistance was found approximately 4.07 k-ohm. So, the conductivity increased and retained the same value of the original sample. The PL spectroscopy in multiple points was done to determine the defect state of the annealed sample (Fig 3.34).

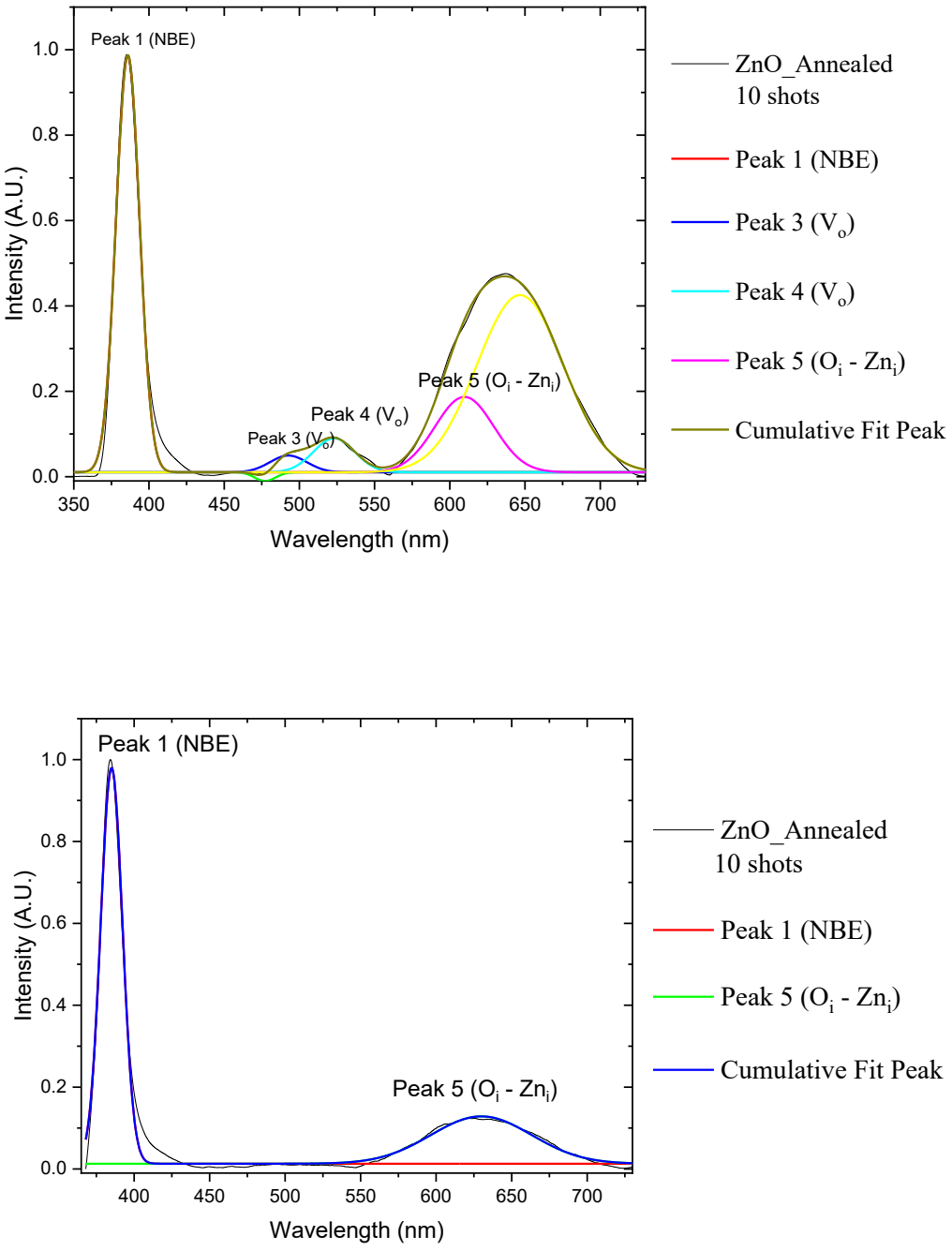

Fig 3.34: PL spectroscopy of annealed ZnO (10 shots)

From the PL spectroscopy, it is evident that the intensity of the NBE emission at ~390 has been increased further and the deep level defects have been decreased. In the first graph the peaks 493 and 523 nm can be attributed to the single charged and +2 charged Oxygen vacancies. The peak at 477 nm is missing in the second graph but present in the first one, so recombination of Zn interstitial (Zn_i) with Zn vacancies (V_{Zn}) in a small amount is there. There are also Zn interstitials present in the sample and it recombines with few oxygen interstitials hence gives rise to the peak at ~609 nm in the second graph. In the PL spectra, the intensity of NBE emission is higher than the Deep level emission, which suggest that the film has fewer surface defects. Also, the deep level defects have been increased in few spots, which was countered by the absence of the defects in some other spots, keeping the conductivity same as the original sample. The X-Ray Diffraction pattern didn't show any change after annealing with 10 shots (Fig 3.35). The variation of resistance with different number of laser shots are given in table 3.

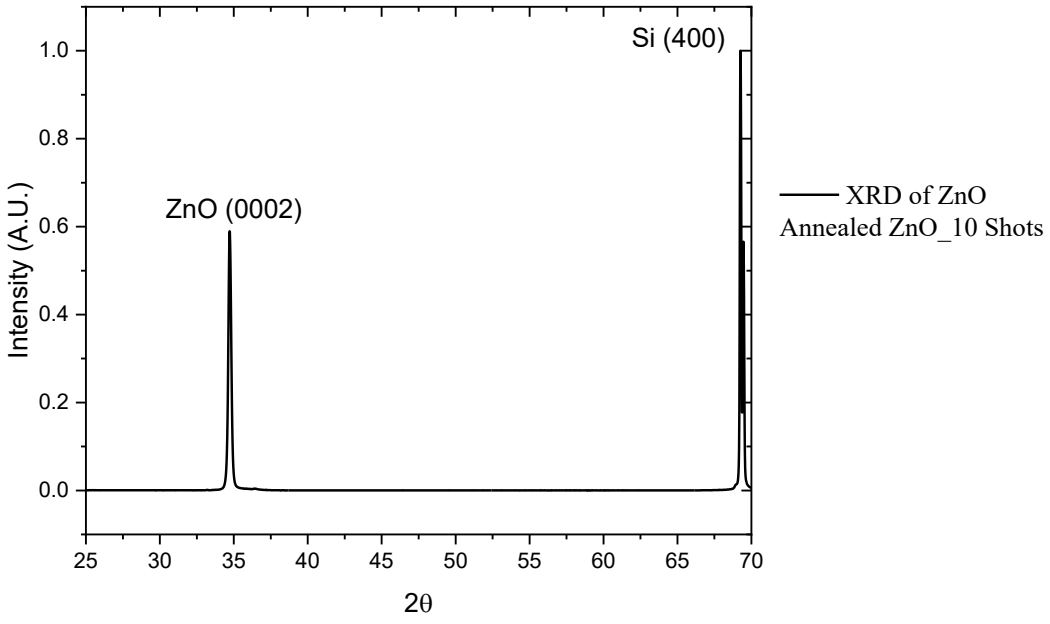

Fig 3.35: XRD of annealed ZnO with 10 laser shots

Table 3: Resistance of the samples at different annealing steps

Sample	Resistance (in K-ohm)
ZnO_Pure	4.08
ZnO_annealed (2 shots)	5.17
ZnO_annealed (7 shots)	4.85
ZnO_annealed (10 shots)	4.07

It can be concluded from this experiment that modification of electronic conductivity is possible using pulsed laser Annealing. It was also determined that the main reason behind the low conductivity is the rise of Oxygen Vacancy. While the last annealing step provided defect free region, it also provided regions with more V_o than the original sample. And as a result, the conductivity remained same of the original one. We suspect that, more balanced distribution of laser energy is required to have a uniform effect in the whole sample.

CONCLUSIONS

ZnO thin films have been grown on different substrates with pulsed laser deposition technique. Pulsed laser Annealing was carried out by varying the laser parameters and a suitable value for minimizing the defects was determined. SEM/EDX images revealed that no significant damage was done while the sample was irradiated with laser shots. The X-Ray diffraction and Raman spectroscopy was done, and no change was observed due to annealing. The modification of the defects was determined with photoluminescence spectroscopy. The measurements revealed how the native point defects such as vacancies and interstitials diffuse into the structure, change the level of energy, transform from one charged state to another, change the recombination between them due to laser annealing. The I-V measurement showed how the conductivity changes with the modification of defect states and mostly the oxygen vacancies are responsible for low conductivity. Though in our experiment it was not possible to decrease the defects to a point where conductivity is maximized, the findings gave insightful information about the native point defects and probably with some modification in the technique used for the experiment will yield better result. In the future, hall measurement can be done to find the mobility, and transistor I-V characterization can be done for thin film transistor applications.

REFERENCES

[1] A. Janotti and C. Walle, Rep. Prog. Phys. **72**, 126501 (2009)

[2] Ü. Özgür, Ya. I. Alivov, C. Liu, A. Teke, M. A. Reshchikov, S. Doğan, V. Avrutin, S.-J. Cho, and H. Morkoç, J. Appl. Phys. **98**, 041301 (2005)

[3] M. D. McCluskey and S. J. Jokela, J. Appl. Phys. **106**, 071101 (2009)

[4] A. Kobayashi, O. F. Sankey, and J. D. Dow, Phys. Rev. B **28**, 946 (1983)

[5] K.-K. Kim, J.-H. Song, H.-J. Jung, W.-K. Choi, S.-J. Park, and J.-H. Song, J. Appl. Phys. **87**, 3573 (2000)

[6] R. J. Lad, P. D. Funkenbusch, and C. R. Aita, J. Vac. Sci. Technol. **17**, 808 (1980)

[7] S. W. Jung, W. I. Park, H. D. Cheong, G.-C. Yi, H. M. Jang, S. Hong, and T. Joo, Appl. Phys. Lett. **80**, 1924 (2002)

[8] T. P. Smith, H. A. McLean, D. J. Smith, P. Q. Miraglia, A. M. Roskowski, and R. F. Davis, J. Electron. Mater. **33**, 826 (2004)

[9] A. Mang, K. Reimann, and St. Rübenacke, Solid State Commun. **94**, 251 (1995)

[10] W. R. L. Lambrecht, A. V. Rodina, S. Limpijumnong, B. Segall, and B. K. Meyer, Phys. Rev. B **65**, 075207 (2002).

[11] S. Vempati, J. Mitra and P. Dawson, Nanoscale Research Letters, **7**, 470 (2012)

[12] P. Dahan, V. Fleurov, P. Thurian, R. Heitz, A. Hoffmann, and I. Broser, J. Phys.: Condens. Matter **10**, 2007 (1998).

[13] S. Y. Lee, E. S. Shim, H. S. Kang, S. S. Pang, and J. S. Kang, Thin Solid Films **473**, 31 (2005).

[14] C. M. Wang, L. V. Saraf, and Y. Qiang, Thin Solid Films **516**, 8337 (2008)

[15] O. Vigil, L. Vaillant, F. Cruz, G. Santana, A. Morales-Acevedo, and G. Contreras-Puente, Thin Solid Films, 53 (2000)

[16] X.M. Fan, J.S. Lian, Z.X. Guo and H.J. Lu, Appl. Surf. Science, **239** (2005)

[17] J. M. Carlsson, H. S. Domingos, P. D. Bristowe, and B. Hellsing, Phys. Rev. Lett. **91**, 165506 (2003)

[18] D. M. Fonz and A. L. Shluger, Phys. Rev. B, **99**, 014202 (2019)

[19] G. Xiong, J. Wilkinson, M. Mischuck, S. Tuzemen, K. B. Ucer, and R. T. Williams, Appl. Phys. Lett. **80**, 1195 (2002)

[20] C. Park, J. Lee and W. S. Chang, J. Phys. Chem. C, **119** (2015)

[21] S. E. Nikitin, Yu. A. Nikolaev, I. K. Polushina, V. Yu. Rud, Yu. V. Rud, and E. I. Terukov, Semiconductors **37**, 1329 (2003)

[22] B. P. Zhang, N. T. Binh, Y. Segawa, Y. Kashiwaba, and K. Haga, Appl. Phys. Lett. **84**, 586 (2004)

[23] A. Ohtomo, M. Kawasaki, T. Koida, K. Masubuchi, and H. Koinuma, Appl. Phys. Lett. **72**, 2466 (1998).